Microfabrication Methods for the Study of Chemotaxis

by

Maiya Shur

B.S. Mechanical Engineering (2002)
B.S. Biology as recommended by the Department of Biology (2002)
Massachusetts Institute of Technology

Submitted to the Department of Mechanical Engineering
in Partial Fulfillment of the Requirements for the Degree of
Master of Science in Mechanical Engineering

at the
Massachusetts Institute of Technology
May 7, 2004

Signature of Author.....
Department of Mechanical Engineering
May 7, 2004

Certified by.....
C. Forbes Dewey, Jr.
Professor of Mechanical Engineering and Biomedical Engineering
Thesis Supervisor

Accepted by.....
Ain Sonin
Chairman, Department Committee on Graduate Students

Microfabrication Methods for the Study of Chemotaxis

by

Maiya Shur

Submitted to the Department of Mechanical Engineeing
on May 7, 2004 in Partial Fulfillment of the
Requirements for the Degree of Master of Science
in Mechanical Engineering

Abstract

We have developed a system for studying chemotaxis in a microfabricated system. The goal was to develop a system capable of generating spatially and temporally stable concentration gradients of a chemotactic molecule while providing a viable environment for the cell. Numerical models were generated to investigate fluid flow in microchannels for given geometries. Through computational modeling and experimentally-driven iteration of the design, features of the chamber were determined and geometry was established. Prototypes of the system were fabricated using soft lithography and multi-layer soft lithography techniques. Three fluid delivery methods for establishing gradients in the system have been studied: gravity feed system, dual-syringe pump feed system, and integrated individually-controlled peristaltic pump feed system.

We were able to create spatially and temporally stable gradients using the dual-syringe feed setup. Two syringes were used to pump a chemokine and a buffer in parallel channels that are connected by a cross-channel and terminated to a single output. Microbeads in the flow were used to confirm the lack of movement in the cross-channel.

Human neutrophil viability over the course of several hours and directed cell movement was demonstrated in microchannels.

Thesis Supervisor: C. Forbes Dewey, Jr.
Title: Professor of Mechanical Engineering and Bioengineering

Acknowledgements

Special thanks to Professor Dewey for his able guidance, patience and support. Thank you to Alex Rabodzey for his help with the cell biology portion of the thesis. Thank you to Kurt Broderick at MTL for the training and help with the microfabrication. Thank you to Jennifer Blundo and Belinda Yap for their helpful advice. Finally, many thanks to Chan Young Park, whose brief participation in the project proved instrumental to its success.

Thank you to my parents, grandparents and all of my friends for their moral support and helpful advice.

This research was funded in part by NSF and DARPA.

Table of Contents

List of Figures

1.0 Background

1.1 Chemotaxis: Why is it important?

Many cells have the ability to sense the direction of external chemical signals and respond by polarizing and migrating towards chemoattractants or away from chemorepellants. This phenomenon, called chemotaxis, has been shown to play an important role in embryogenesis, neuronal growth and regeneration, immune system response, angiogenesis, and other biological phenomena [1]. In addition, cell migration is also important for emerging technologies such as tissue engineering and biomedical implants. This simple behavior is apparently mediated by complex underlying mechanisms that have been the focus of many studies and models.

A common feature of chemotactic signaling systems is the ability to adapt to different levels of external stimuli, so that it is the gradient of the signaling molecule rather than the magnitude of the signal that determines the response. Cells exhibiting perfect adaptation respond to spatially homogeneous increases in external stimulus by transient activation of specific transcellular signaling pathways. The same signals can be inactivated if the signal present is spatially inhomogeneous and graded [2].

Once the cell detects the source of the signal, it orients itself in the direction of the gradient. The motility of a eukaryotic cell in the direction of a gradient starts with polarization which is the development of leading and trailing edges. Polarization involves changes in cell morphology and asymmetrical distribution of multiple proteins and lipids leading to complete internal cell reorganization. The cell also forms F-actin-filled lamellopod, fillapod and pseudopod extensions and retractions, as a means of moving the body [3]. The sensing of the gradient and the coordination of movement of the cell involves regulation of complex

intramolecular interactions. More than 60 families of actin regulatory proteins have been implicated in the regulation of the extending pseudopod. The complexity is further increased if one accounts for a multitude of processes involved in cell locomotion, such as regulation of the microtubule cytoskeleton, interaction of the cell with the extracellular matrix, changes in ion channel distribution. Actin and actin-binding proteins are localized on the leading edge. Other molecules, such as conventional myosin, accumulate at the trailing edge. Unpolarized cells maintain equal sensitivity throughout their surface. Directional sensing refers to the cell's ability to detect an extracellular gradient, accumulate signaling molecules, and initiate polarization responses. When a chemotactically sensitive cell is exposed to a shallow gradient, slight differences in receptor occupancy across the surface of the cell lead to polarization. In polarized leukocytes, the trailing edge is more sensitive to chemoattractants than the leading edge. This allows the cell to sense a change in the direction of the gradient and change its direction [4].

The ability to observe a single cell's response to a chemotactic environment is necessary in order to validate numerical models and describe chemotactic behavior mathematically. To date, several methods of studying chemotaxis have been developed. Most of these methods fail to establish linear, time-invariant, spatially-stable gradients.

1.1.1 Dunn Chamber Assay

The Dunn chamber assay is currently widely used by biologists to create temporary gradients [5]. The Dunn chamber consists of two concentric wells that are micromachined into a glass slide. The wells are typically 250 μm deep. Between the two wells is a 20 μm deep bridge. See Figure 1.1.1 for a schematic of the Dunn Chamber.

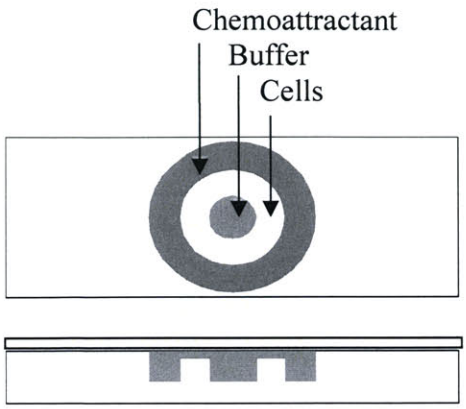

Figure 1.1.1: Schematic of the Dunn chamber for studying chemotaxis.

Wells are filled with buffer solution and cells are plated onto the cover slip which is then inverted onto the glass slide. A chemoattractant is then added to the outer well and the entire chamber is inverted to be viewed under a microscope. An approximately linear gradient is established after about an hour of stabilization time and then decays over several hours, with half-life of decay estimated to be several hours.

A major drawback of the Dunn chamber assay is the method with which cells are delivered into the system. Upon inversion of the glass slide, cells that are plated outside of the well areas are squished on contact. Presumably, this causes the release of chemotactic agents, enzymes, lysozymes and organelles contained in the cell's cytoplasm. Their effect, if any, on the viable cells in the chamber cannot be quantified. Furthermore, the gradient in the chamber, while approximately linear on the length scale of the cell, decays over time. This makes it difficult to mathematically describe the extent of the gradient at any point in time, and correlate that to the behavior of the cell. Additionally, compared to microfabrication methods, the Dunn chamber uses relatively large volumes of reagent. However, the Dunn chamber continues to be one of the most widely used methods of studying chemotaxis for its simplicity of operation and low cost of manufacturing.

1.1.2 Whitesides Chemotaxis Study

Whitesides, et al, reported having created a method for generation of complex gradients using microfluidic networks. In the device, streams of laminarly flowing fluid generated step concentration gradients perpendicular to the direction of flow. The gradients that were created using this method were spatially and temporally stable because the solutions are continuously renewed [6]. Figure 1.1.2 shows the mask layout of a 3-input / 9-output microfluidic network used for generating gradients.

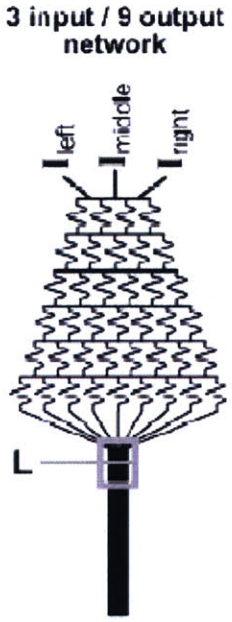

Figure 1.1.2: Mask layout. [7]

The three incoming channels at the top are driven by a syringe pump to deliver 3 different concentrations of reagent. To create a linear gradient, the outer channels carry fluid with normalized concentrations of 0 and 1 of the reagent. The middle channel carries reagent at a concentration of 0.5. To create a bell-shaped gradient, the middle channel carried a concentration of 1 while both outer channels carry concentrations of 0. As streams of liquid travel down the network of channels, they are continuously split and recombined at the nodes, and allowed to mix by diffusion in the serpentine channels. At the end of the network, all

streams converge in a broad channel. The initial step profile of concentration at the inlets of the broad channel blurs due to diffusion.

Since diffusion is slow relative to the time required to move through the channels, the concentration gradient perpendicular to the direction of flow is maintained in the broad channel. Because solution is continuously renewed in the system, the gradient is stable in a given section of the broad channel.

Several such networks can be connected in parallel to create periodic gradients. The devices are distinct until joined together in the broad channel, thereby allowing the creation of complex saw tooth, sinusoidal, or double parabolic gradients. The usefulness of creating complex gradients in the broad channel is questionable, as their resolution is magnitudes greater than the length scale of a single cell.

Another advantage of such combining these networks is the ability to superimpose gradients of reagents. Overlapping gradients provide a means of studying the role of competing gradients in chemotaxis.

Because of the configuration of the branched network, the larger the distance of the nodes form the vertical symmetry of the axis, the network, the higher the order of the branched system, and the larger is the amount of a stream that is diverted to the outer branches of the network. This bias to the outer channels determines the shape of the concentration profiles at the outlet.

1.1.3 Manson Chemotaxis Study

Manson, et al, reported the development of a versatile microfluidic assay for studying bacterial chemotaxis. The device shown in Figure 1.1.3 contains an inlet for chemoeffectors, an inlet for buffer and an inlet for bacteria.

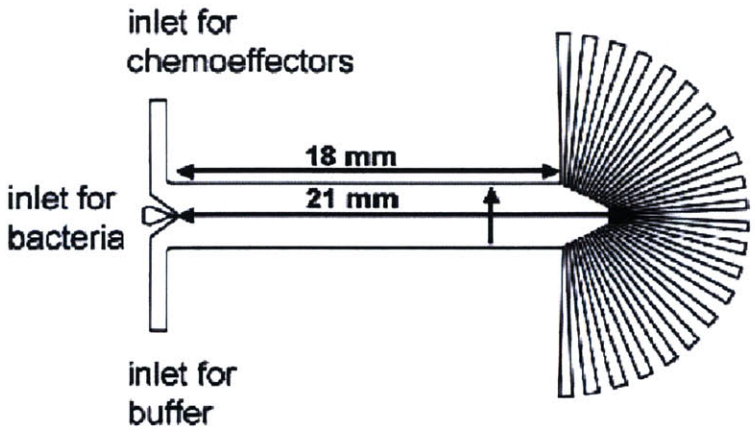

Figure 1.1.3: Device for microfluidic bacterial chemotaxis. [8]

The main channel is 3.18mm wide and 8μm tall, and has a total volume flowrate of 314 nl/min (velocity of 1.23 cm/min). Therefore a cell moving with the bulk flow would take 1.71 minutes to travel the length of the 2.1 cm long channel. The flow exits at 22 200 μm-wide output channels. The bacteria move down the length of the channel with the bulk flow, but also traverse the width of the channel in the direction of an increasing chemotactic signal. The bacteria are collected at the output channels according to the extent of its migration normal to the direction of flow. The distribution of cells can then be correlated to the magnitude and gradient of the chemoattractant in the flow [8].

Because of the dynamic nature of the gradient and the method for collecting the data, the only cells which can be studied in such a manner are bacterial cells, which can swim in the chemotactic gradient by propelling themselves with flagella. Other chemotactic cells of interest cannot be studied in such a manner, as they need to be attached to a substrate in order to move.

Some of the shortcomings of this assay include the limited distance and time over which a single cell can be observed. Another drawback is the spatially changing gradient. According to the PNAS publication, "The slope of the gradient, monitored with fluorescent dyes, was six times as steep immediately downstream of the inlets as it was in the region immediately

upstream of the outlets." While it is still possible to observe the qualitative effects of chemoeffectors on bacterial movement, the dissipating gradient makes it difficult to draw quantitative conclusions from the data.

Another potential drawback of the design is the pressure bias to outlets that may result from blockages of outlets by exiting cells, or non-uniformities due to the manufacturing process. Such a bias can distort the gradient in the chamber and even pull cells to and from outlets other than the one that they reach chemotactically.

1.1.4 Other Assays

Other methods of studying chemotaxis include the Boyden chamber and its modifications and using pipettes to release chemoattractants near plated cells. The modified Boyden chamber assay is used to study chemotaxis of leukocytes or other migratory cells. The apparatus consists of two multi-well chambers separated by a filter containing pores of uniform size. A solution containing a chemotactic factor is placed in the bottom chamber and a cell suspension is placed in the upper chamber. Cells migrate through the pores, across the thickness of the filter, and toward the chemoattractant in the lower chamber. Cells that migrated across the filter and attached to the underside are counted. Data are often expressed in terms of a migration Index: the number of cells that migrated in response to the chemokine relative to the number of cells that migrated randomly, in response to the buffer only.[9] The gradient in the Boyden chamber is not stable.

The problem with generating gradients using pipette methods is that gradients evolving from point sources and line sources have exponentially decaying concentration profiles. These assays rely on the fact that on the cellular level the gradient at any point is approximately linear.

However, when a cell is tracked over a large distance, the change in concentration between two points is hard to quantify and correlate to the cell's movement. This time-variant approach to studying chemotaxis yields only reliable qualitative results and requires complex mathematical modeling to in order to estimate the parameters of chemotaxis.

2.0 Microfabrication

This thesis explores microfabrication as a method of rapid-prototyping and constructing a device for studying chemotaxis. This section gives a general overview of microfabrication methods, and a more detailed introduction to the soft lithography methods used in this thesis work.

2.1 Overview

Microfabrication has become an important tool in biological experimentation. The convergence of microfabrication technology and biology has made possible high throughput techniques that require relatively small volumes of analytes and reagents.

Soft lithography uses elastomeric materials to fabricate the patterned elements by molding. Poly(dimethylsiloxane) (PDMS) and other siloxane-based polymers are widely used in making structures for soft lithography. PDMS has a number of properties that make it suitable for creating structures. It is moderately stiff, with a Young's modulus of 1 MPa. It is non-toxic and biocompatible. It is optically transparent down to ~300 nm[10]. It is also hydrophobic (Θ_a^{H20} = 110°) but can be briefly converted to a hydrophilic form (Θ_a^{H20} ~ 10°) by plasma treatment. Contact of two oxidized PDMS surfaces results in irreversible contact adhesion caused by a spontaneous dehydration of the SiOH groups. Treatment of the master with an

alkyltrichlorosilane ($RsiCl_3$) introduces R groups onto the PDMS surface, reducing interfacial free energies and thus reducing adhesion [11].

PDMS is also relatively permeable to nonpolar gases, such as O_2, N_2 and CO_2, allowing the devices to be used for cell culture [12].

The patterns to be molded in photoresist can be designed using commercial computer drawing programs. The designs are then printed onto transparencies using a commercial printer. These transparencies are used in place of chrome masks in contact photolithography, thereby reducing the cost and production time dramatically. With this technique, dimensions as small as 50μm can be created with high fidelity. It is possible to make features that are up to 25 times smaller than the features printed on the transparency by using microscope projection lithography, whereby a microscope lens is used to reduce the image. Among the drawbacks of photolithography is that the control over surface structure is limited, compared with some other microfabrication techniques.

Other competing technologies for making masters are laser ablation, ultra-precision CNC machining, precision EDM, silicon wet bulk micromachining, deep reactive ion etching (DRIE). These methods are serial processes and are rather slow compared with photolithography, but are capable of producing more controlled surface finish and higher resolution of features. CNC machining is appropriate for making features larger than 50μm [13].

2.1.2 Multilayer Soft Lithography

The multilayer application of soft lithography combines soft lithography techniques with the capability to bond patterned layers of the elastomer. The technique uses separately patterned features which are aligned to form a device with built in valves and pumps. A top layer has an

excess of the curing agent and the bottom layer has an excess of the elastomer base. First the two layers are undercured separately, and the top layer is removed from the wafer and aligned onto the bottom layer. Because each layer has an excess of one of the reagents, reactive molecules remain on the surface and bond irreversibly upon further cure when the two surfaces are brought into contact. The resulting three-dimensional structure is therefore monolithic. Figure 2.1.2 is a schematic overview of the fabrication process.

A typical flow layer may contain channels that are 100 μm wide and up to 10 μm deep; the aspect ratio is restricted to 10:1 by the polymer's tendency to sag. A control layer may contain channels that are 100 μm wide, and when two layers are crossed, the area of the resulting valve is 100 μm x 100 μm. Because the flow layer is typically spin-coated onto the wafer, the membrane of polymer between the two layers is relatively thin. Because of the low Young's modulus of the elastomer, microstructures can be actuated with small forces. When sufficient pressure is applied to the control layer channel, the membrane deflects downward, completely closing the flow channel with zero dead volume. A 100 μm x 100 μm valve has a response time of 1 ms, can operate at up to 100 Hz. An actuation pressure of 100 kPA is sufficient to completely occlude the channel [14].

Because the pressure required to fully occlude a flow channel strongly depends on the area of the valve membrane, it is possible to have a control line of 50 μm passing across several flow channels and only actuating at an area where the control line widens to 100 μm [15].

In order to close completely, the flow channel must be rounded at the top. Square channels do not close completely, and backflow can occur past the corners. A post-processing to remelt the photoresist is carried out to achieve rounded corners.

Using three valves in series, and operating in a 100, 110, 010, 011, 001, 101 pattern of open (0) and closed (1) valves, creates a peristaltic pump that can achieve maximum flow rate of 2.35 nl/sec. Maximum pumping rate is attained when actuating between 75 Hz and 200 Hz. The valves and pumps do not show any sign of wear or fatigue after more than 4 million actuations, or ~11 hours of operation at 100 Hz [16].

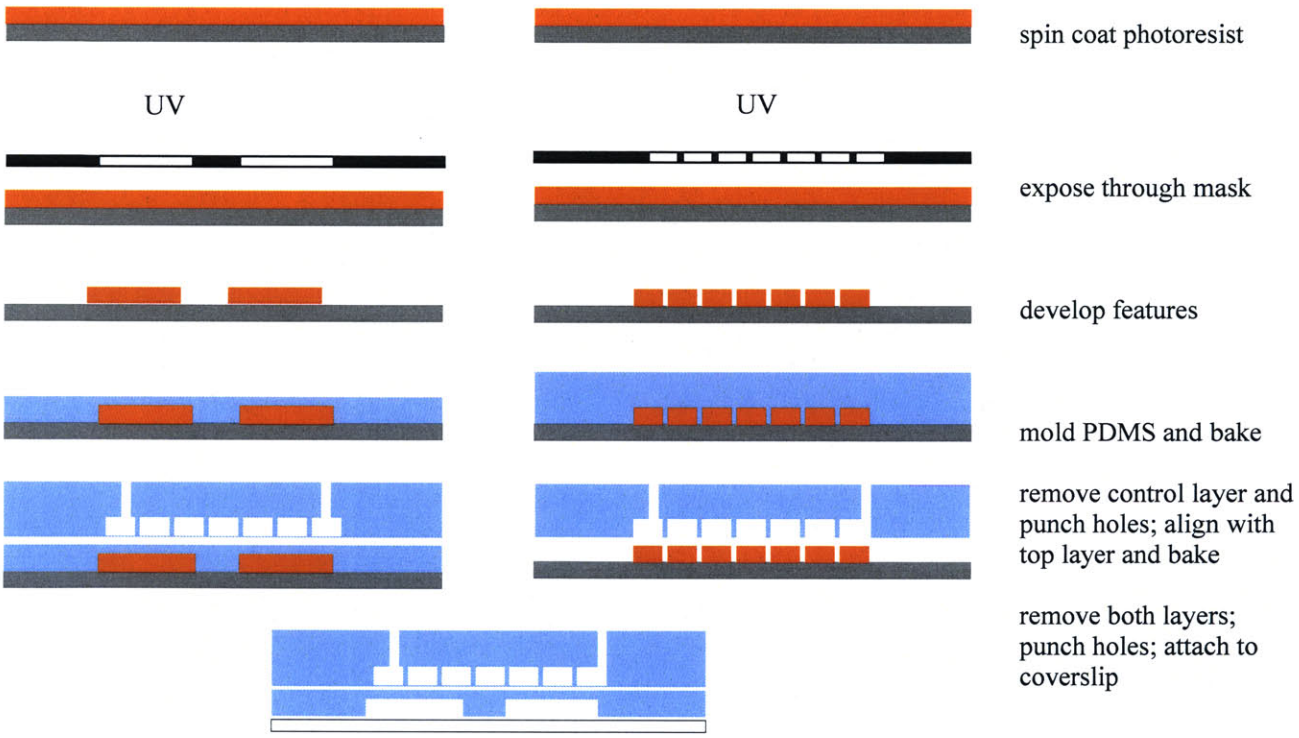

Figure 2.1.2: An overview of the fabrication process. Adapted from [16]

2.1.3 Soft lithography in biology

The ability to position cells on a surface, to control their spacing and study them in a single-cell environment has been made possible by soft lithography techniques. Isolating cells on a surface makes it possible to study events occurring in each individual cell instead of relying on statistical distributions of a population of cells. By eliminating cell-cell interactions,

individual response of cells to the environment can be observed. Alternatively, several cells can be patterned together in a monolayer such that interactions between them can be studied in a controlled environment.

The ability to deliver controlled amounts of reagents to single cells makes it possible to study the influence of the reagents on the behavior of the cells in a highly controlled manner. The laminar flow of fluids in microchannels can be used to deliver reagents in different concentrations across a cell. A cell placed at the interface of two or more streams and partially treated with reagent reveals localization effects in the cell [12].

Surfaces can be patterned through fabrication methods to change their texture. Wettability can be changed through chemical modification. Small molecules can be patterned on a surface by using fluid flow.

This thesis work has employed microfabrication techniques for generating temporally and spatially stable gradients in microchannels. Device geometry has been determined, and several methods of delivering reagents have been investigated. The devices that have been fabricated it possible to study cell migration, proliferation, development and differentiation that, in vivo, occur along a gradient.

3.0 Theoretical Modeling

In order to investigate the effects of device geometry on the system, a FLUENT computational model was developed. Parameters such as width, height and aspect ratios were varied, and flow velocities and pressures were calculated. Oxygen diffusion from the atmosphere and species diffusion in the cross-channels were also calculated.

3.1 Geometry and Dimensions of Chamber

The flow layer of the chamber consists of two parallel channels. One channel is used to deliver a chemokine in buffer, while the other channel is used to deliver buffer with a fluorescent tracer to monitor the gradient. (Eventually, fluorescently labeled chemoattractants could be used to monitor the gradient chemokine molecule directly) The perpendicular channel connecting the two parallel channels serves as a flow observations area. Balancing the pressures at the entrances to the perpendicular channel, and thereby preventing any pressure-driven flow in the channel, allows for only diffusive transport of species to occur in the cross-channel, and therefore a gradient to form down the length of the channel.

For the multilayer process, the limiting factor in determining the dimensions of the chamber was the resolution of the AZ process. The 10:1 aspect ratio used to prevent sagging of elastomer limited the width of the channels to 100 μm.[1]

In the multi-layer fabrication, the control layer consists of two independently-controlled peristaltic pumps, and one valve, as shown in Figure 3.1.1. While it is possible to design a more compact device, the spacing between the inlets is necessary to accommodate the air and solution tubing, and keep the tubing out of the light source of the microscope.

Alignment markers are needed in order to position the control layer on top of the flow layer during the molding process. In addition, distance markers are placed at even intervals along the flow channel in order to assist in qualitative assessment of the extent of the gradient and the positions of cells in the chamber.

[1] Upon testing the device, it became obvious that further scaling is needed to prevent obstruction of flow channels by cells. 18 μm devices were manufactured in AZ photoresist. It is, however, possible to manufacture devices with heights up to 200 μm when different formulas of AZ photoresist are used.

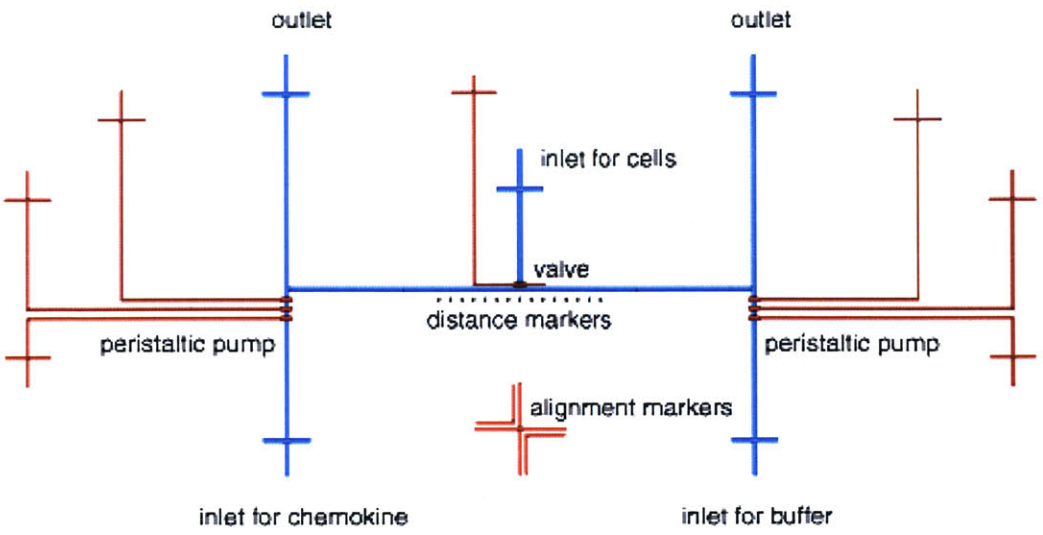

Figure 3.1.1: Layout for overall mask design. The features shown in blue constitute the bottom (flow) layer. The features shown in red are the top (control) layer.

A total of 6 devices can be patterned onto a single wafer as shown in Figure 3.1.2.

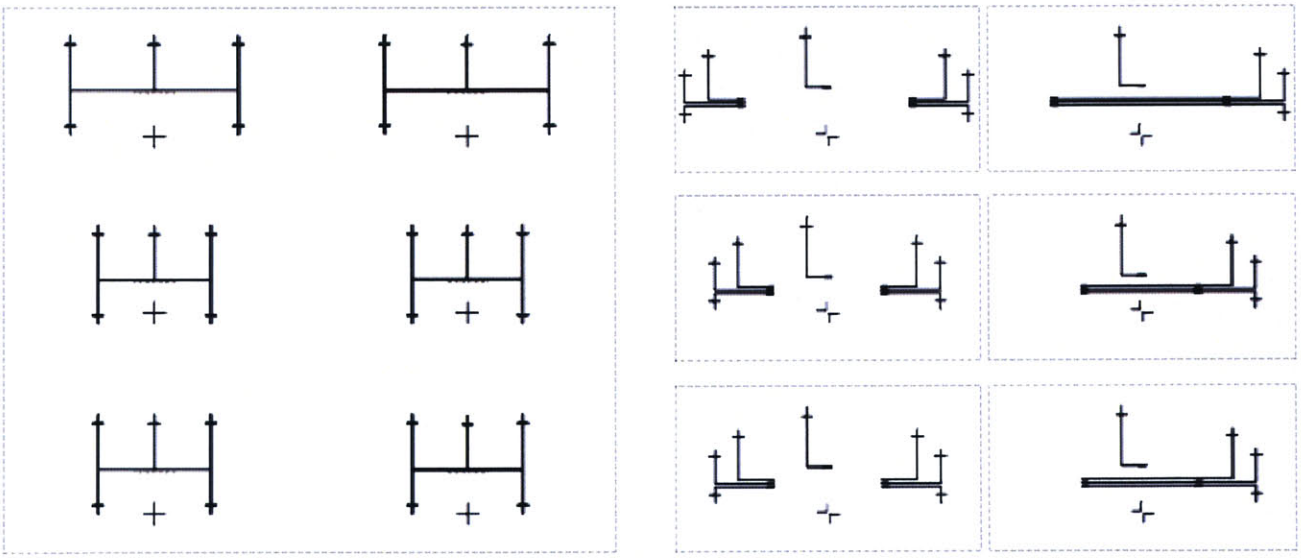

Figure 3.1.2: Layout of a 6-device mask for positive photoresist process. Features for the flow layer (left) and features for the control layer (right) are patterned onto separate wafers. The control layer features are scaled about center of each device. The dashed lines are printed in order to facilitate cutting out and aligning the devices.

The single-layer process, for which external methods of driving the fluid are used, did not require rounded channels. Therefore, an AZ photoresist process is no longer necessary and higher aspect ratios can be achieved using SU-8 photoresist. The mask design can be scaled up to make cross-channels around 50 μm wide by 50 μm tall and outer channels as large as 500

microns wide. Sufficiently increasing the ratio of widths of outer channels to cross-channel keeps the fluid flow in the main channels. This is because the resistance to flow in the main channels is significantly lower than that in the cross-channel.

The GE Handbook gives the resistance in a rectangular channel as a function of viscosity, channel length and channel dimensions:

$$R = \frac{\mu L(b+c)^2}{8(bc)^3}\left[96 - 95\frac{b}{c} + 56\left(\frac{b}{c}\right)^2\right]$$

where c is the width of the channel, b is the depth of the channel. In our device, the cross-channel is square (50 μm x 50 μm) and the side channel is rectangular (500 μm x 50 μm). Therefore, $b_1 = b_2 = c_1$ and $c_2 = 10c_1$. Using this in the above expression, we find that $R_1 = 28.5(\mu L/b^4)$ and $R_2 = 1.32(\mu L/b^4)$; the resistance to flow in the cross-channel is more than 20 times greater than the resistance in the side channels. Resistance also increases linearly with length, so shorter channels offer less resistance to fluid flow.

When holes are punched in PDMS at the inlets to the channels, the placement of the hole affects the length of the channel by as much as a millimeter. The effects of this on the resistance can be quite pronounced, and care must be taken to punch holes as symmetrically as possible.

Given the number of factors that affect the total resistance of a channel and lack of methods to quantify the extent of the manufacturing defects, it is impossible to create a unified model of the conditions in the channels in order to determine the optimum geometry. However, such a model is not necessary, as the ultimate goal is to achieve a velocity and pressure balance between two parallel flows connected by a cross-channel, an effect that is readily observed experimentally. Through experimentally-driven iteration of the design, it was determined that a 10:1 ratio of channel width was sufficiently large to balance pressures between the outlets and

prevent fluid flow through the cross-channel. Furthermore, by increasing the area of the outer channels, the velocity is minimized for a given volume flowrate. Lower velocities in the outer channels allow lower pressures in the system, and therefore easier balancing of pressure across the cell channel.

Initial tests to determine geometry for the channels revealed that when the cross-channel is oriented perpendicular to the parallel flow channels, flow becomes easily diverted at the junction. Orienting the cross-channels in the opposite direction of the bulk flow prevents the diversion of the flow to the cross-channel. The inertia of the bulk flow in the wider channel carries the fluid toward the outlet.

Initially, a mask was designed having two inlets and two outlets. Through experiments, it was determined that faster convergence of two outlet channels further reduced the imbalances in the system. When working on the scale of micrometers, small defects that are present due to fabrication become highly pronounced and affect flow distribution. Therefore, it is desirable to have the smallest possible distance that the fluid must travel within the chamber. See Section 3.2 for further discussion and a numerical assessment of the problem. In addition, having two separate outlets requires having two outlet pieces of tubing which must be the same length and fixed at the same height in order to balance gravitational pressures at the outlet and the resistances of the tubing.

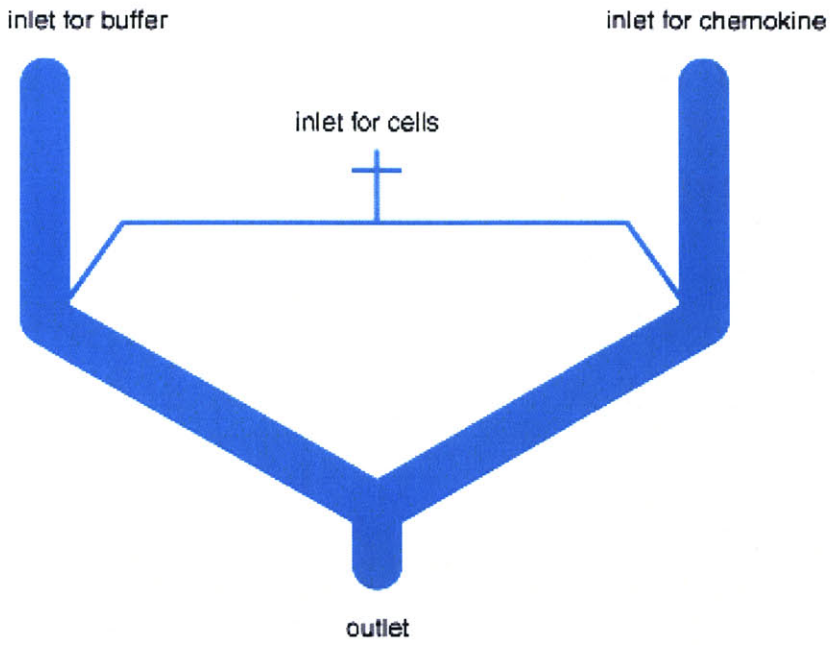

Figure 3.1.3: Layout for the single layer design consists of two inlets, a cell-loading line and one outlet. The ratio of cross-channel width to main channel width is 10:1.

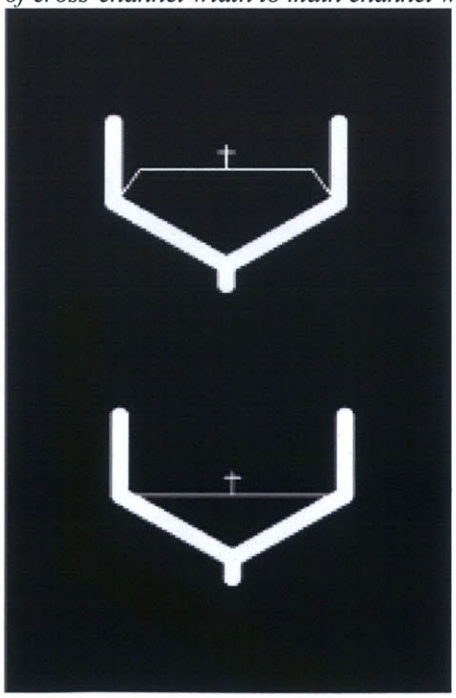

Figure 3.1.4: An example of a mask layout for the SU-8 process. The features are patterned on a transparency in white on black. Since these devices are significantly smaller than the AZ multi-layer pattern and don't require any alignment features, as many as 10 devices can fit onto one 3" wafer.

Once the cells are placed in a chemotactic gradient, their movement prevents the chamber from truly achieving steady state conditions. A leukocyte moving at 20 μm/minute [Devreotes] can traverse the half a 10 mm cross-channel length in 2 hours. The presence of cells in the cross-channel increases the resistance to the flow by reducing the effective area of the channel. However, this effect is less pronounced in the channels that are 50 μm tall, than in those that are 10 μm.

3.2 Fluent computational model of flows and pressures

Fluent, a finite element fluid computational software package, was used to calculate pressures and velocities in the channels and to investigate the effect of defects and the presence of cells on the fluid flow. A model of the simple channel layout geometry was created using GAMBIT 2.1. Inputs and outputs were designated and the model was imported into Fluent. A finite element mesh was created, initial conditions were set and solutions were iterated to find pressure distributions and corresponding velocities of the fluid in the channels.

Fluent was used to investigate the effects of manufacturing defects and presence of cells in the multi-layer geometry. This investigation was carried out because these effects are highly pronounced in the restricted geometry of the multilayer device, where the dimensions are limited by the manufacturing process. The only way to overcome the imbalances in the multilayer system is to vary the flowrate supplied by the peristaltic pumps.

A perfectly symmetrical channel will have no flow in the cross-channel, resulting in the following pressure distribution:

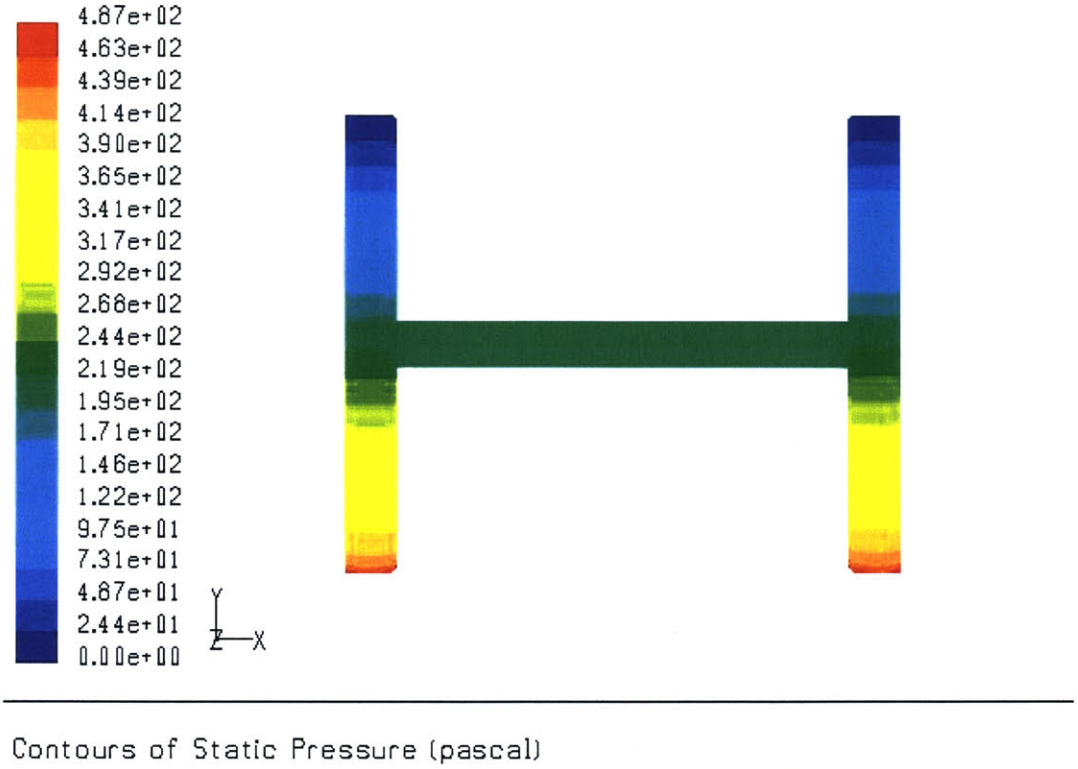

Figure 3.2.1: Pressure distribution for the symmetric geometry with no defects. Input velocity at the inlets is .0023 mm/sec, corresponding to the highest flowrate achievable by embedded peristaltic pumps.

However, when working with devices of 10-μm height, defects due to fabrication have a profound effect on the pressure distribution. Since pressure varies as the square of the velocity in the channel, $P \propto v^2$, and imbalance in the velocities at the inlets to the cross-channel results in a pressure-driven flow across the channel. When $Q_1/A_1 = Q_2/A_2$, the velocities in the two channels will be equal. However, a 10% constriction or expansion in surface area in one of the channels will result in a directly proportional difference in velocity in that area. Therefore, the input flowrate must also be changed by 10%. However, when features are scaled up by a factor of five, the fabrication defects are no longer as pronounced.

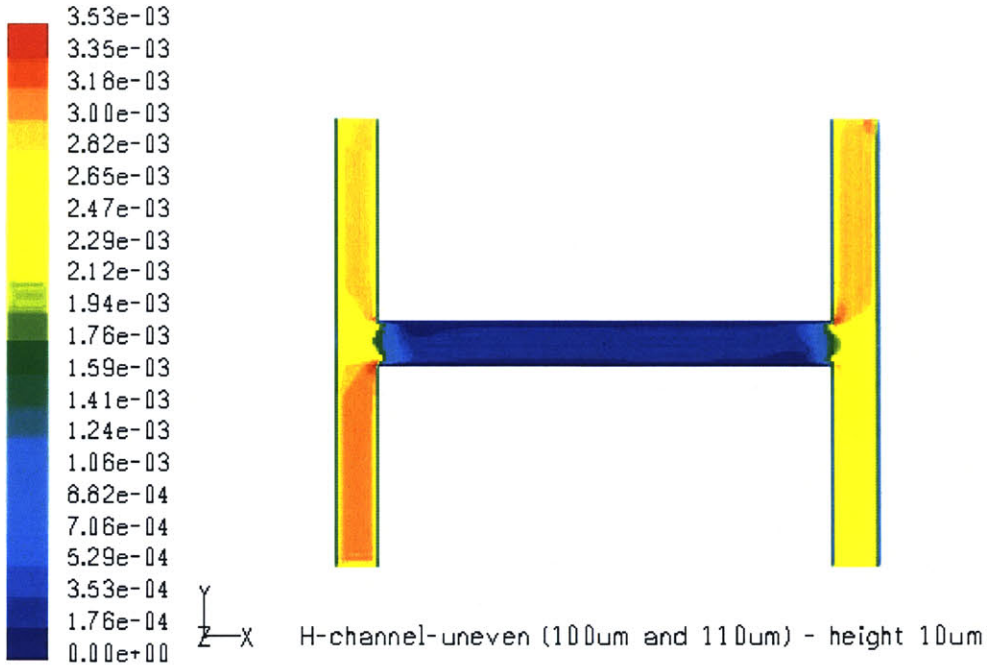

Figure 3.2.2: This figure shows the effects of a cross-sectional area variation of 10% between the two parallel channels.

The effects of the presence of cells in the cross-channel were also investigated using FLUENT modeling. Figure 3.2.3 is the graphic output of the FLUENT simulation when two cells are placed into the cross-channel. The cells were modeled as 4μm-tall (10μm on the side) protrusions in the side-wall of the cross-channel, typical of the dimensions of an adhered cell. It can be seen from Figure 3.2.3 and the corresponding graph of velocity magnitudes in figure 3.2.4 that the presence of cells results in a flow in the cross-channel.

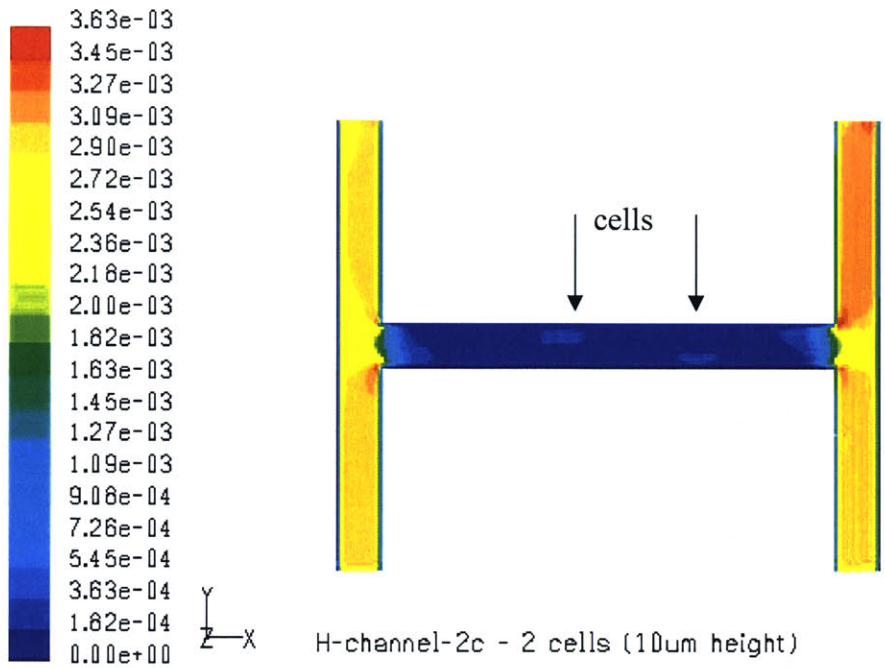

Figure 3.2.3: The figure shows the effect of the presence of two asymmetrically-placed cells in the cross-channel.

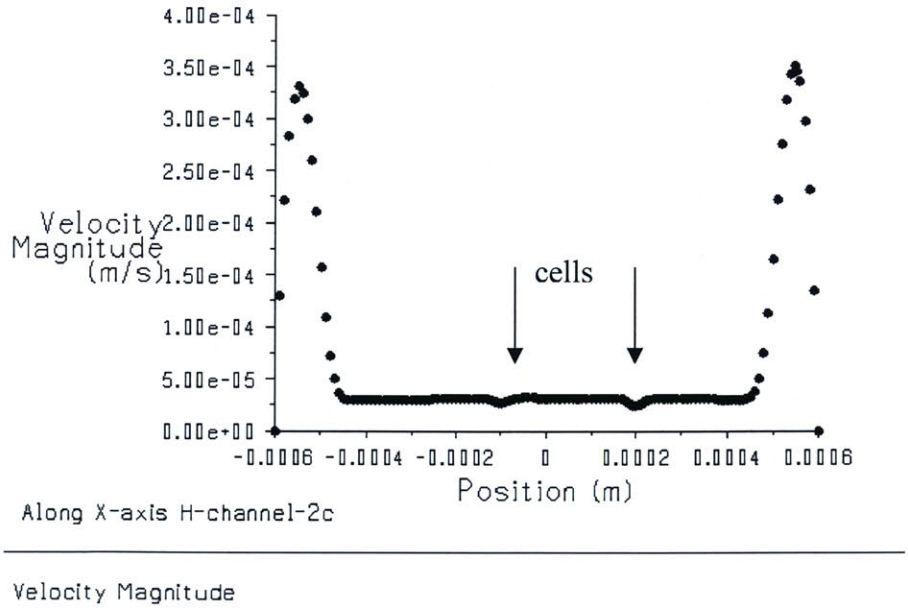

Figure 3.2.4: Plot of the velocity distribution across the middle of the cross-channel from Figure 3.2.3. Local effects in the flow can be observed due to the presence of the cells.

Since the velocity is on the order of 10^{-6} m/s, the flow in the cross-channel is faster than the diffusion of species such as rhodamine or fluorescein that is used as a means of detecting the gradient; the input flowrates must be controlled separately and adjusted to balance the pressures on the two sides using individually-controlled peristaltic pumps.

3.3 Diffusion of Species

Diffusion of species occurs on a timescale given by, $\tau = l^2/D$. For a small molecule such as rhodamine, the coefficient of diffusion, D = 4.37 x 10^{-10} m^2/sec. Therefore, rhodamine diffuses at the rate of ~21 μm/sec. For a cross-channel that is 5mm long, the time to traverse the entire channel is ~4 minutes. The time to set up a gradient in the channel is realistically even shorter given that the cross-channel can be pre-filled with rhodamine.

In simple channels with smooth walls, low *Re* pressure flows are uniaxial and laminar. So any mixing that occurs between the flows is purely diffusive. The convection vs. diffusion of species is characterized by the Péclet number ($Pe = Ul/D$, where D is the molecular diffusivity). In a channel that is 500 μm wide by 50 μm tall, and a flowrate Q = 10 μL/hr, the velocity U = .112 mm/sec. For a small molecule of D = 3 x 10^{-10} m^2/sec, Pe = 185. Given Pe, the mixing distance can be calculated as $\Delta y_m \sim Ul^2/D = (Pe)l$ [17]. For the given system, Δy_m = 9.25 cm. This mixing distance is prohibitively long, and therefore mixing by diffusion is not feasible to achieve for such large channels, at the low flowrate. This calculation is relevant for the future versions of the integrated chamber where reagents can be mixed to desired concentration right on the chip.

3.4 Oxygen transport

Single cell studies in PDMS devices have shown that cell survival rates are comparable to those in regular cell culture. Since PDMS provides an oxygen permeable barrier between air and fluid, sufficient amount of oxygen diffuses to the cells through the membrane. However, for studying cell monolayers in PDMS devices, it is necessary to determine whether enough oxygen diffuses through the membrane to the fluid and the cells at the bottom of the channel. Using the Film model (at steady state), as represented in Figure 3.4.1, a differential equation can be formulated:

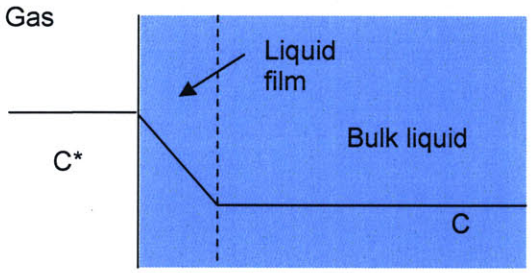

Figure 3.4.1: Film model for gas diffusion through fluid.

When cells are present at the bottom of the chamber, and are consuming oxygen at a steady rate, their consumption rate and the change in concentration with time can be formulated as

$$dC/dt = k_L a\,(C^* - C) - OUR$$

where a is the specific surface area per unit volume [cm^{-1}], C (and C*) is the oxygen concentration [g/L] and k is the mass transfer coefficient [cm/s]. The quantity $k_L a$ is volumetric oxygen transfer coefficient, which indicates the maximum oxygen uptake rate (OUR):

$$OUR_{max} = k_L a\, C^*$$

The maximum oxygen limited cell density (OLCD) can be determined by using the oxygen consumption rate, Q_{O2}.

When concentration of oxygen at the bottom is 0, the OUR is assumed to be at a maximum. The following equation for the concentration varying with distance and time can be written:

$$\partial C(x,t)/\partial t = \partial/\partial x(D\ \partial C(x,t)/\partial x) - OUR$$

The profile of oxygen concentration is linear in PDMS and quadratic in water. The assumptions are that no liquid film layer exists and diffusion rate is dominated by diffusion through the PDMS layer.

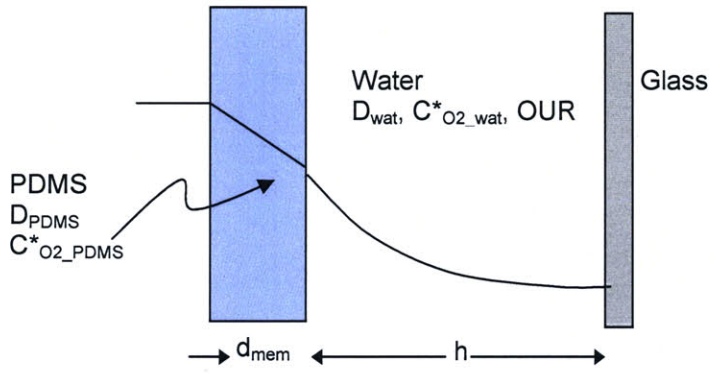

Figure 3.4.2: Oxygen diffusion in PDMS channel of height, h, and membrane thickness d_{mem}.

Solving the differential equation and applying appropriate boundary conditions results in the following expression for the volumetric oxygen transfer coefficient:

$$k_L a_{eff\_unmixed} = 1/(\ h^2/(2*D_w) + K*d_{mem}*h/D_p\ )$$

where K is the ratio $C_{satWater}/C_{satPDMS}$, D_p is the diffusion coefficient of O_2 in PDMS, D_w is the diffusion coefficient of O_2 in water, h is well height, and d_{mem} is the thickness of the PDMS membrane.

Using appropriate values for the variables, and plotting $k_L a$ vs. well depth, the following set of curves (for thicknesses of PDMS between 100 and 500 μm) can be obtained.

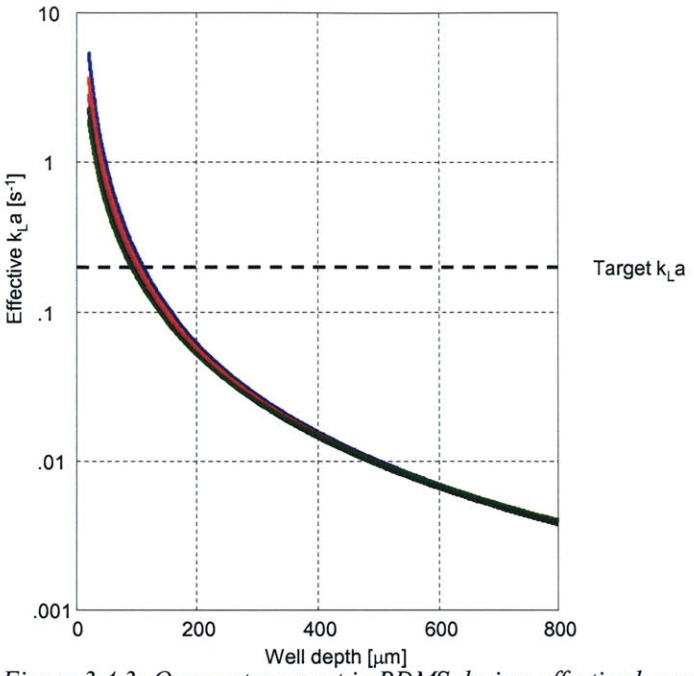

Figure 3.4.3: Oxygen transport in PDMS device: effective k_La vs well depth

As seen in Figure 3.4.3, the well depth has the most profound effect on the oxygen transport in the channels. Channels of ~150 μm are around the desired k_La, as compared to microtiter plates and bench-top bioreactors, and will be able to sustain high density cell growth. This will not be the case for channels of increasing depth if diffusion is relied on for oxygen delivery. For deeper wells, an alternate method of oxygen delivery should be used.

4.0 Materials and Methods

4.1 Overview

Microfluidic devices were fabricated in poly(dimethylsiloxane) (PDMS) using one-layer and two-layer soft lithography techniques. A mask was printed at high resolution and used to pattern silicone wafers to create features in photoresist. These features are the used as a negative master for forming positive replicas that produced channels in an elastomeric material. The devices were sealed to glass to create enclosed channels.

4. 2 Mask design

The mask was created in Adobe Illustrator 8.0 with the maximum resolution setting of 9600 dpi. For the single layer application, a negative mask was printed to be used with negative photoresist: the features were white on black. All features were scaled by 1.7% to account for shrinking of elastomer following curing and release from the mold [13].

For the multilayer application, the control and the flow layer of the device were created together, and markers were created to facilitate the alignment of features during fabrication. The control layer was scaled in Illustrator by 1.7%. The features were printed in solid black to be used with positive photoresist.

The masks were printed on transparency at 2540 dpi setting by Mikacolor (CA). It was found that the 2540 dpi setting was an acceptable trade-off between quality and cost of mask, for prototyping purposes.

The flow layer and control layer masks were printed separately, to be patterned onto separate wafers. A 3" silicone wafer can be used to pattern six multi-layer or ~9 single-layer devices. Figure 3.1.1 shows the mask layout for the final design of the device.

4.3 Photolithography

The photolithography step of the fabrication was conducted in the Microfabrication Technology Laboratories' EML (level 100) clean room facility. NPN mech grade silicone wafers (Silicon Quest, CA) were rinsed with acetone, methanol, and iso-propanol and dried with compressed nitrogen gas. The wafers were then dehydrated for 30 minutes at 130°C in an oven.

4.3.1 Positive-Resist Photolithography

The wafer was centered on top of the vacuum chuck of the spin-coater and treated with the adhesion promoter HMDS.

Shipley AZ4620 photoresist (Clariant, CA) was spin-coated to 10μm height by ramping up 0-500 rpm in 5-10 seconds, 500-1000 rpm in 5 seconds, and holding at 2000 rpm for 60 seconds. (For 20 μm height, the photoresist was spun at 800 rpm). Because the EML facility lacks a programmable spin coater, the ramping was done manually, so the given times were approximated. This caused slight variability of thicknesses between wafers.

The wafer was soft-baked at 90°C on the hotplate. The mask transparency was then placed, emulsion side down, on top of the coated wafer, and secured with a glass square. The wafer was exposed to UV light for 30 seconds at 4 $mJ/cm^2/sec$ and then developed in AZ440 developer solution for approximately 4 minutes followed by a rinse in developer solution diluted 5:1 with water. To expedite the diffusion-limited development process, the wafer was agitated in a non-repetitive manner during development. Any photoresist remaining on the sides of the wafer was removed using an acetone-soaked swab. The wafer was then rinsed with deionized water and dried with nitrogen gas.

In an alternative process which produced better results, the wafer was post baked at 90°C for 30 minutes in an oven. Following the soft-bake, the wafer was exposed for 30 seconds in 3 intervals of 10 seconds on and 10 seconds off. The features that resulted were less likely to come detached during the development process, and there was virtually no cracking in the photoresist. This may be attributed to the fact that with interval exposure, the photoresist does not overheat.

The developed wafer was then dehydrated on the hotplate at 90°C to remove excess moisture. The fidelity of the features was observed using a microscope. Width and height of the features was confirmed using a profilometer. See Figure 4.3.1 for an example of profilometry output for a wafer patterned with six valves.

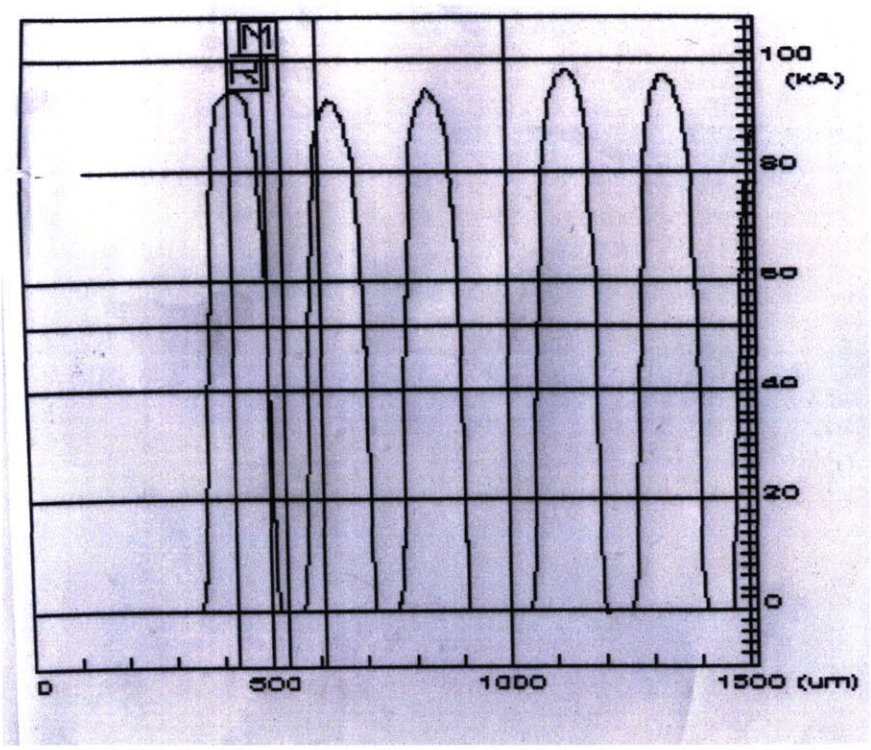

Figure 4.3.1: Profilometer output for 6 valves patterned on a wafer. Rounded curves occur due to the shape of the profilometer tip.

4.3.2 Multilayer soft lithography

Corners of the flow layer features were rounded in order to facilitate efficient opening and closing of the valves. This was done by placing the wafer on the hot plate set at 300°C for 3-5 seconds. This temperature is just below the boiling point of the polymer, and allows for a quick remelt and rounding of the channels.

The wafers were exposed to a vapor of tridecafluoro-1,1,22-tetrahydrooctyl-1-trichlorosilane (United Chemical Technologies, PA) for 60 seconds by placing in a closed container with the highly volatile liquid. The silane precipitates onto the wafer surface in a monolayer and passivates it, allowing for easy removal of cured elastomer. The silanizing should be done approximately every 3 times that a mold is made from the wafer.

The wafers patterned with control layer features were placed in Petri dishes lined with aluminum foil. Sylgard 184 (DowCorning, MI) PDMS was mixed in two batches of 20:1 and 5:1 elastomer to curing agent ratios. The PDMS was mixed and degassed by spinning in the THINKY centrifuge. Approximately 25 mL of the 5:1 PDMS : elastomer mixture was poured onto each wafer and placed into the oven at 80°C.

After 18 minutes, the semi-cured elastomer was cut out and peeled off the wafer. Inlet and outlet holes were punched using a 23 gauge luer stub needle adapter. The control layer pieces were washed with isopropanol and dried by spraying with nitrogen gas.

The 20:1 elastomer was spin-coated onto the wafers patterned with flow layer features. The wafers were placed into the oven at 80°C. After 17 minutes the wafers were removed from the oven. The flow and control layers were superimposed with the help of alignment markers under the stereo microscope. The wafers were placed back into the oven for an hour to ensure a full cure. Curing the two layers together causes mixing at the interface and creates covalent bonds between the two layers.

The wafers were then removed and the flow layer (with the control layer on top) was cut out and peeled from the wafer. Holes for the flow layer were punched through both layers from the bottom up using a 23 gauge luer stub needle adapter. The devices were washed with isopropanol and dried with compressed nitrogen.

The devices were then sealed to glass cover slips by activating the PDMS and the glass in air plasma (600-800 mTorr, 30 sec) and joining the surfaces together. Plasma treatment results in irreversible sealing by a process in which the Si-OH groups formed by the plasma condense to form Si-O-Si [18]. See Figure 4.3.2 for a schematic of the sealing process.

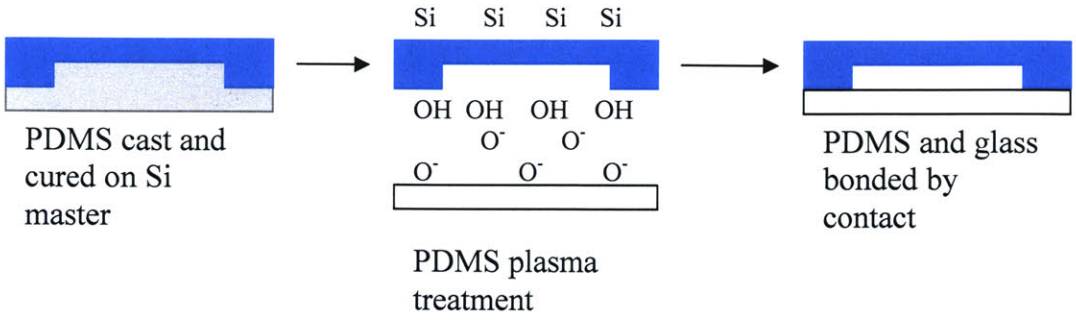

Figure 4.3.2: plasma treatment and sealing process

Polyethylene tubing of .02" ID and .06" OD was connected to 23-gauge needles (New England Small Tube Corp.) and inserted into the inlet holes. No tubing was inserted into the outlet hole and reagent was allowed to pool at the outlet. This made it easier to clear the system of air bubbles.

4.3.3 Negative-Resist Photolithography

For devices with wider and taller features, SU-8 (Microchem, MA) negative photoresist was used in the fabrication of the mold. The following process describes the fabrication of 50 μm-tall features. For other processes refer to recipes and suggestions at www.microchem.com. SU-8 is the most commonly used process with the near UV (350-400nm) radiation. Upon exposure, cross-linking proceeds in two steps: formation of strong acid during the exposure process, followed by acid-initiated, thermally driven epoxy cross-linking during the post-exposure bake.

SU-8 50 photoresist was dispensed onto cleaned (see Section 4.3) and dehydrated wafer at 1 mL of resist per inch of substrate diameter. Photoresist was spin-coated at 500 rpm for 10 seconds to spread the resist to edges of wafer, and then ramped up at 300 rpm/second and spun at 2000 rpm for an additional 30 seconds. Wafers were then pre-baked on a hotplate for 6 minutes at 65°C, followed by 20 minutes at 95°C. These values are given for direct contact heating. The

EML hotplates are coated with Aluminum foil and therefore do not provide direct contact between hotplate and substrate. In the future, it may be desirable to calibrate the wafer temperature for EML hotplates in order to more rigorously adhere to the recommended protocol. To reduce stresses in the photoresist, wafers were allowed to cool slowly before exposure. Wafers were exposed to UV light continuously for 60 seconds at 4 $mJ/cm^2/sec$. High energy wavelengths below 350 nm were filtered out by placing a piece of quartz into a filter slot of the broadband mask aligner. To reduce bowing caused by the cross-linking of the photoresist, the wafers were post-baked for 1 minute at 65°C, then 5 minutes at 95C, and allowed to cool slowly. Wafers were developed with sprayed PM Acetate while spinning at 2000 rmp. It was found that this method of development reduced lift-off of features that occurs in a bath of developer solution. The wafer is then washed with iso-propanol and dried with nitrogen. If a white film remains on the wafer, the development is not complete.

Profilometry data are not available on features taller than 30 μm. Resulting surface and edge roughness is comparable to that of the AZ process prior to remelt, but its effects are less pronounced because of the scaled-up geometry of the device, as discussed previously.

4.3.4 Single-Layer Soft Lithography

Wafers were pretreated with TCMS vapor. PDMS elastomer base and curing agent were mixed in 10:1 ratio and degassed in the THINKY centrifuge. PDMS mold was poured and baked at 80°C for 20 minutes. Because no post-development bake/remelt step is done in the SU-8 process, the roughness of the features traps air bubbles at the edges and angles of the master. The trapped air bubbles can be eliminated by poking with a thin needle.

Holes were punched using a 23-gauge luer-stub adapter. Devices were cleaned with iso-propanol, dried with nitrogen and sealed to glass slides following activation with air plasma, as previously described.

4.4 General Comments on Fabrication Process

We were not able to achieve very good feature resolution using the photolithography setup in the EML. Features as large as 50 μm came out rugged at the edges, with edge defects of around several microns. This may be due in part to the "dirty" wafers with a layer of epitaxial oxide that were used for processing.

The AZ photoresist degrades after multiple molding attempts and features wear off after approximately 10 molds are made from the wafer.

It is important to complete the molding process in a single day. The 5:1 elastomer will fully cure at room temperature over the course of a day, and the layer mold will no longer bond to the 20:1 flow layer mold.

Doing the molding step in the non-clean room environment introduces airborne particles onto the PDMS surface. These pollutants can interfere with the optical clarity of the device and the adhesion properties of the layers. Their effects are minimized by washing surfaces with iso-propanol and working quickly, but some particles remain embedded between the layers of the device. The EML facility does not have the proper degassing and programmable spin-coating equipment, so this processing cannot be done there.

As of this step, the multi-layer molding of the devices is a relatively low-throughput process. Of the 6 multi-layer devices that can be patterned on a single wafer, about 5 usually survive all of the steps.

4.5 Neutrophil Isolation and Injection

Neutrophils were isolated from human blood at the Hartwig lab at the Brigham and Women's Hospital. 10mL of blood was drawn into a syringe prefilled with 1 mL of anti-coagulant. ~5mL of dextran/3% PBS solution was drawn into the syringe. Syringe was inverted for 30 minutes to allow red blood cells to coagulate, leaving a frothy coat of leukocytes in plasma on top.

The frothy coat was transferred to a 15 mL falcon tube and centrifuged at 3000 rpm for 10 minutes. Supernatant was aspirated and cells were resuspended with a small volume of HBSS. Remaining red blood cells were lysed by adding 10 mL of deionized water and shaking the 15 mL tube for 2-3 seconds and immediately adding 1 mL of 10x PBS solution to restore osmolarity. The cells were then centrifuged again at 5000 rpm for 3 minutes. Supernatant was aspirated and cells were resuspended in .1M glu, .3% BSA in HBSS. If red blood cells were still present, cells were transferred to a 50mL falcon tube and shocked with 45mL of DI water, immediately adding 5 mL of 10x PBS to restore osmolarity, centrifuging, aspirating and resuspending.

FMLP (formal met-leu-pro), a well-characterized chemotactic molecule that binds the 7-spanning G-protein-coupled receptor on the surface of neutrophils [19], was diluted to .1μM in HBSS/BSA solution. Neutrophils were exposed to a $2x10^{-5}$ M/μm gradient of FMLP and tracked over the course of several minutes that it took them to migrate to the exit of the cross-channel.

Gradient formation and steady-state was tracked by taking images at 30-second intervals and comparing the intensities in the range of 500-650 nm (the emission spectra of Rhodamine 110).

5.0 Experimental Setup

5.1 Gravity-Feed Setup

Large reservoir syringes are connected via a three-way valve to smaller priming syringes. The syringes are clamped to lab stands and elevated to a desired height above the device. Controlling the height determines the pressure head and therefore the velocity of the flow through the tubing and the channels. Priming syringes are used to clear the air out of the PDMS device. The valves are then opened to supply chemoattractant and buffer through the tubing to the device. The level of the syringes with respect to each other is manually adjusted until the microspheres in the cross-channel are not moving. Because the level of the fluid in the syringes depends on the velocity of the flow leaving the syringe, which in turn depends on the height of the syringe above the device, the levels in the two syringes are changing at different rates. Therefore, the pressure and, thus, the velocity are constantly changing, leading to an eventual imbalance at the cross-channel inlets. To correct for the changing levels in the reservoir syringes, the syringes are filled to overflow and a syringe pump is used to deliver reagents at a constant rate to the syringes. Presumably, using very large diameter reservoirs results in undetectable changes in the level, and a syringe pump is not required. Figure 5.1 shows a schematic of the setup.

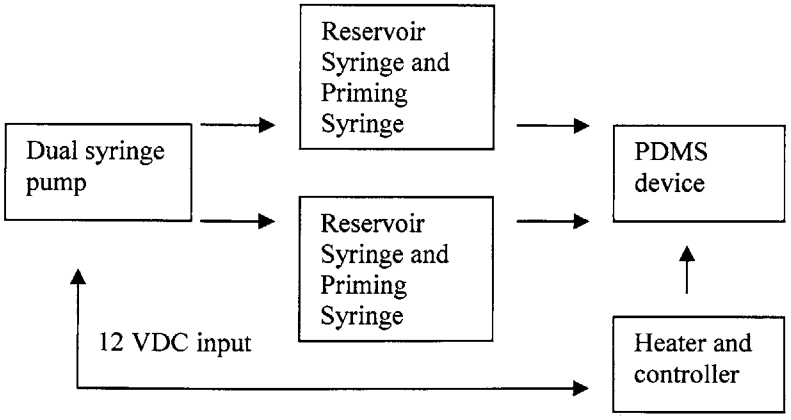

Figure 5.1.1: Gravity feed setup

5.2 Syringe Pump Setup

This simple and robust setup uses a single dual-syringe pump for driving flow through the channels. 25 μL syringes are used in the syringe pumps to reduce the velocity of the flow, and therefore the pressures in the channels, as discussed previously. Figure 5.2 shows the setup.

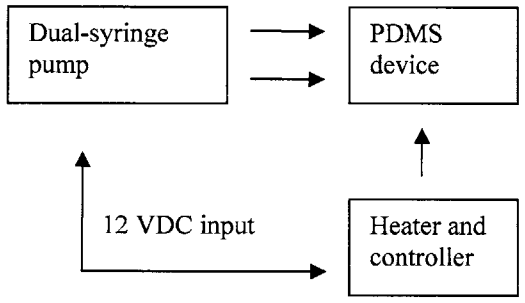

Figure 5.2.1: Syringe pump setup

5.3 Multilayer Application: Controller and Valve Setup

For the multilayer devices, air is supplied to the integrated valves by a set of miniature solenoid valves, whose operation is controlled through the computer.

The control layer consists of two peristaltic pumps and one valve that are actuated by flowing pressurized air through the line. When doing cell work, valves in the control layer are prefilled with water or buffer solution, thereby preventing air diffusion through the valve membrane, dehydration of the chamber and bubble formation in the flow layer.

An array of Lee LHDA12111 solenoid valves (The Lee Co, CT) was used to pressurize the control layer. The Lee valves are attached to a machined air manifold which connects to the lab air (~10-15 psig) outlet. Exceeding these pressures may cause the valves to leak or even become deformed. The valves are controlled through a 25-pin serial BUS cable to a controller board which communicates with the PCI-DIO-32HS data acquisition card (National Instruments, TX) via a SH68-68-D1 shielded cable. LabView 7.0 software was used to program a Virtual

Instrument to write output data to digital lines of the DAQ card. Figure 5.3.1 shows the block diagram of the setup.

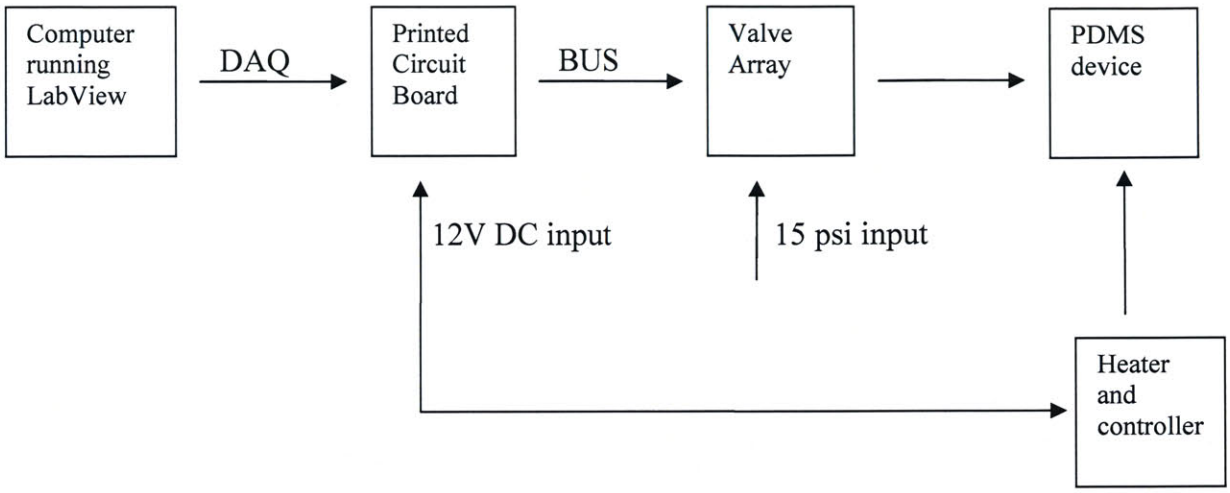

Figure 5.3.1: Block diagram showing the control setup.

Figure 5.3.2 shows the dimensions of the Lee solenoid valves.

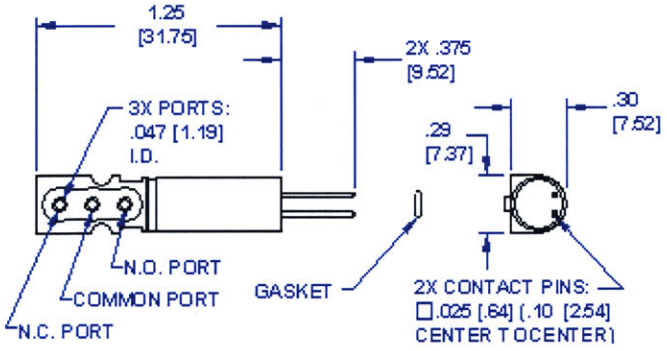

Figure 5.3.2: 3-way solenoid valve

See Figure 5.3.3 for .jpeg image of the solid model of the 8-valve air manifold. See Appendix D for the engineering drawing.

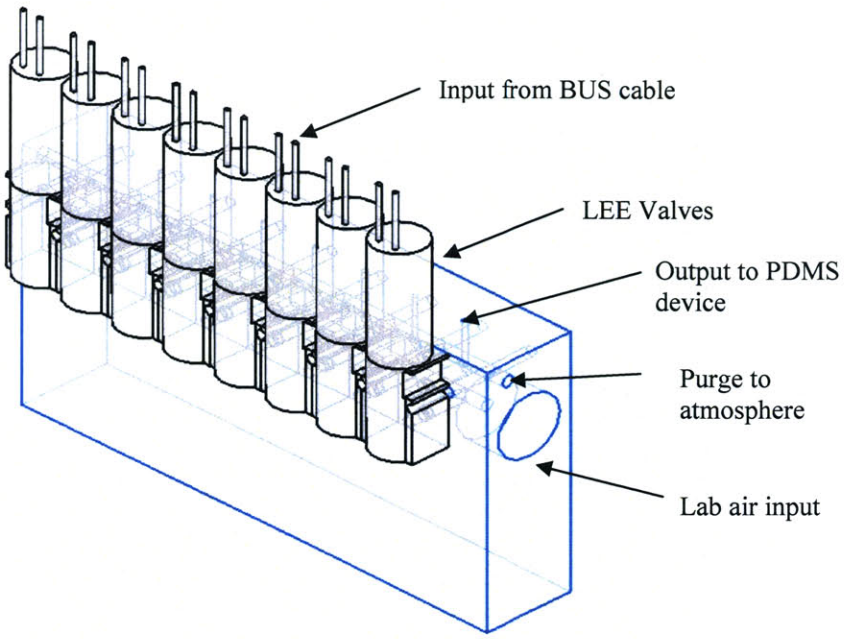

Figure 5.3.3: 8-valve air manifold

The circuit shown in Figure 5.3.4 is used to control each of the valves. The circuit is used to step up the 5V input of the DAQ card and send a 12V output signal to the valves. LabView 7.0 software was used to control the printed circuit board via the DAQ card. The program allows for user input of parameters such as duty cycle, time step and direction of flow for the peristaltic pump control. Each peristaltic pump is controlled separately, allowing the user to adjust parameters while executing the program. The DAQ card which has 64 output pins can be used to control 32 valves independently. In this application, only a total of 7 independent valves were necessary: six valves for two peristaltic pumps and another valve for the cell delivery line.

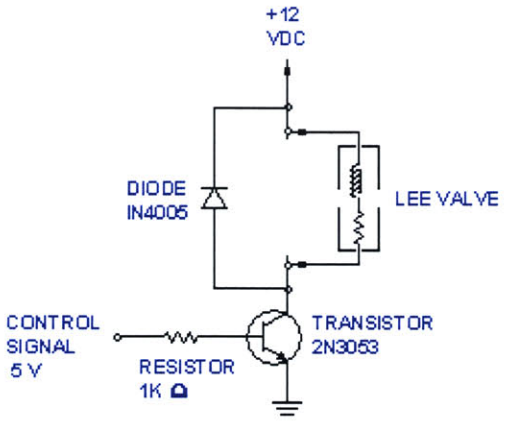

Figure 5.3.4: Basic transistor-diode circuit used for controlling valves.

5.4 Heater and Controller

For the duration of cell experiments, cells must be kept at 36.6°C in order to ensure viability. The CT198 Heaterstat (MinCo, MN) is a sensorless DC temperature controller that uses a high Temperature Coefficient of Resistance (TCR) heater to sense and control heat output, and does not require a separate sensor or thermostat. The CT198 is more durable than a mechanical thermostat due to the solid state electronics, and has an adjustable setpoint which allows you to fine tune the control temperature. The controller maintains the temperature of the heating element, not the heat sink, and therefore requires a higher set-point than the desired temperature.

In order to calibrate the temperature, the heater was placed in contact with a glass slide, a temperature sensor was attached to the opposite side of a glass slide, and the entire setup was placed on a microscope stage to closely simulate experimental conditions. Because the sensor is a strip sensor, it cannot be used to detect temperature inside the channels. Therefore, the calibrated temperature does not account for convective and diffusive losses due to fluid flow in the channels. Better means of monitoring the temperature inside the operating system should be developed if temperature precision is critical to cell viability.

5.5 Microscopy

Images were obtained with 2X, 10X and 20X objectives using the Nikon Eclipse TE2000-U inverted fluorescent microscope. An Apogee Instruments Inc Camera (model X32ME) was used to capture images. Images were modified in MaxIm DL software and resized using Adobe Photoshop 5.5.

Duke Scientific .51 μm fluorescent microspheres were used to image flow profiles and test valve functioning. The spheres contain dyes incorporated into the polymer matrix. The spheres are made of polystyrene, which has a density of 1.05g/cm^3 and a refractive index of 1.59 @ 589nm. Fluorescent images were obtained by exciting the microspheres using a mercury lamp light source, and imaged through a TRITC filter for 1μm spheres and FITC filter for .51 μm spheres.

Fluorescent images for gradient imaging were obtained using a FITC filter to detect Rhodamine 110 in solution.

6.0 Results:

6.1 Gravity-Feed System

Gravity feed was originally discounted as a possible solution to balancing the flows because while the levels could be adjusted initially, a disparity of flow rates in the two inlets would result in an increasing change in height between two lines. Upon further consideration, it was decided that this problem can be solved by filling the reservoirs to the point of overflow and using a syringe pump to keep the reservoirs overflowing. However, such a setup is wasteful, and is not desirable when working with expensive reagents

Given the extremely low flow rates in a gravity-feed system, it was determined that using large reservoirs would make the effects of a change in height over time negligible over the course of a several-hour experiment. Therefore, 10 mL syringes were used as reservoirs.

The following several figures are images of fluorescent microspheres in the gravity feed system. The cross-channel microspheres are not moving across the entire length of the channel. The length of the cross-channel is 5 mm. The following figures show different views and magnifications of microspheres present in cross-channels supplied by gravity feed reservoirs. In Figures 6.1.1 and 6.1.2 the cross-channel and side channels are of equal width. In Figure 6.1.3 the cross-channel : side channel ratio is 1:2. It can be seen in all three images that microspheres in the side channels are moving rapidly while microspheres in the cross-channel do not exhibit directed motion.

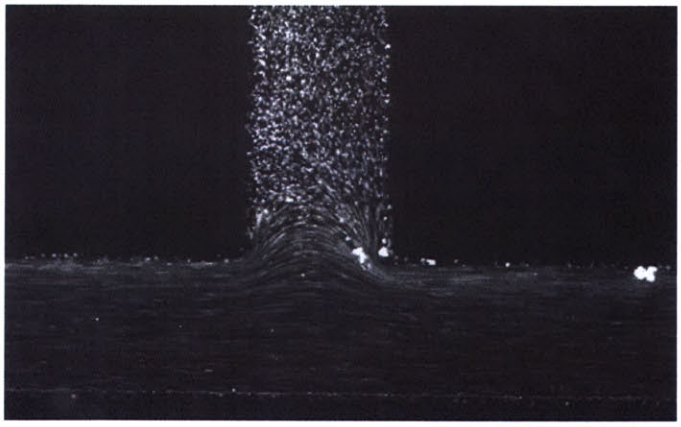

Figure 6.1.1: .51 μm microspheres. The cross-channel and the main flow channels are equal in size (100μm). Exposure time = 0.02 sec

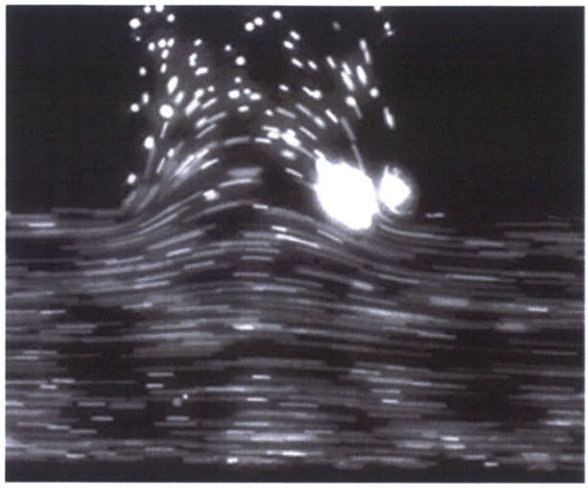

Figure 6.1.2: A 2-fold magnification of image in Figure 6.1.1 Exposure time = 0.04 sec.

Figure 6.1.3: 100x magnification. .51 μm microspheres.

A major difficulty of using the gravity feed setup is the slow response of the fluid system to change. The inertia of the fluid continues to carry fluid in one direction despite a change in pressure. This makes visual feedback difficult and therefore takes a long time to balance the pressures on the sides of the cross-channel. Another drawback of using such a system is that flowrates cannot be determined without knowing the exact height of the syringes above the device.

6.2 Syringe-Pump-Feed System

Initial tests with a dual-syringe pump (Harvard Apparatus, Pump 22) revealed that slow enough flowrates that would result in a pressure balance between the two lines could not be achieved. Next, two separate syringe pumps were used with 3 mL syringes. Because of the large bore size of the syringe, the minimum flowrates (and therefore velocities) achieved with this method were too fast to achieve a balance of pressures. The following figure shows a flow being diverted to the cross-channel when using two 3 mL syringes controlled by two syringe pumps.

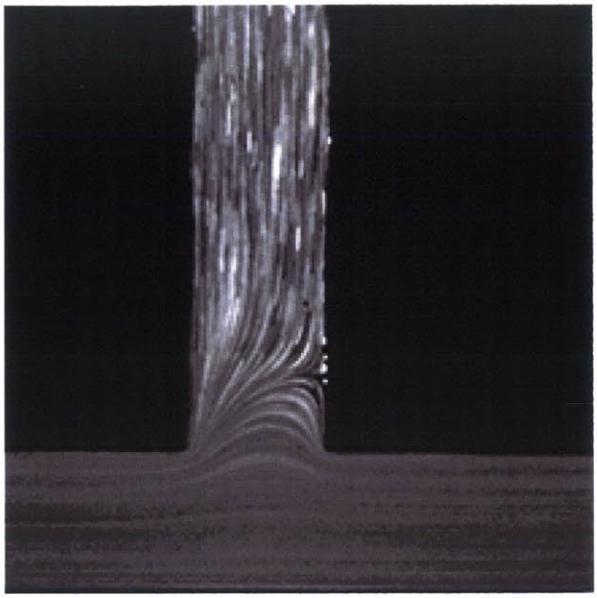

Figure 6.2.1: .51 μm microspheres. Exposure time = 0.02 sec.

While the flow in the cross-channel is slower than the flow in the main channels, any attempts to stop that flow failed. Further tests using two separately-controlled syringe pumps with 25 μL syringes, pumping at lowest possible flowrate (0.073 μL/hr) allowed for a rhodamine gradient to be established. This gradient would typically become dissipated within 10 minutes of operation. Microbeads in the channels did not appear to stand still, as in the gravity-feed system, but slowly traveled back and forth over a distance of several hundred micrometers. This effect could be due to the stepping by the syringe pump motor at extremely low flowrates.

Upon redesigning the channels to have a width ratio of 10:1 (flow channel to cross-channel), it was found that a single syringe pump operating at 10μL/hr with 25μL syringes, was sufficient to balance the pressures in the two lines.

Figure 6.2.2 is a microscope image of the entire device. Rhodamine flown through the channels is used to make this fluorescent image. However, gradients cannot be observed due to the inlets and outlets that flood the area with fluorescence.

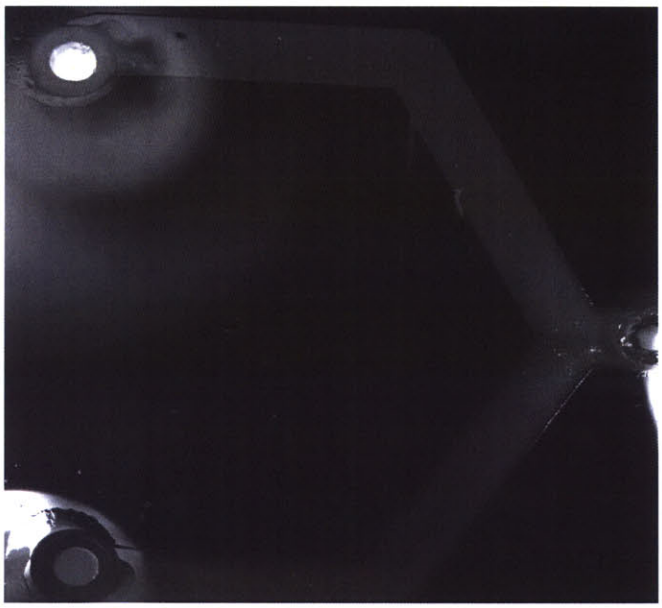

Figure 6.2.2: 20x magnification. Device with rhodamine in the channels.

Figure 6.2.3 shows an image of the entrance region to the device. Beads do not even enter the 50μm cross-channel, unless the channel is primed.

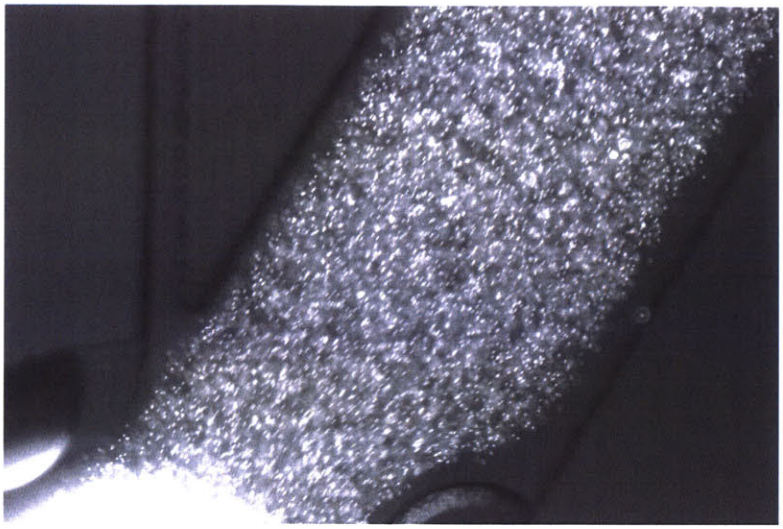

Figure 6.2.3: 100x magnification. Entrance region to the device. The cross-channel on the left is 50 μm wide; the flow channel is 500 μm wide. The device is 50 μm tall.

The following figure shows the cross-channel that has been filled with beads. The beads in the cross-channel exhibit Brownian motion, but no directed movement, while the bulk flow in the large channel is moving to the upper right.

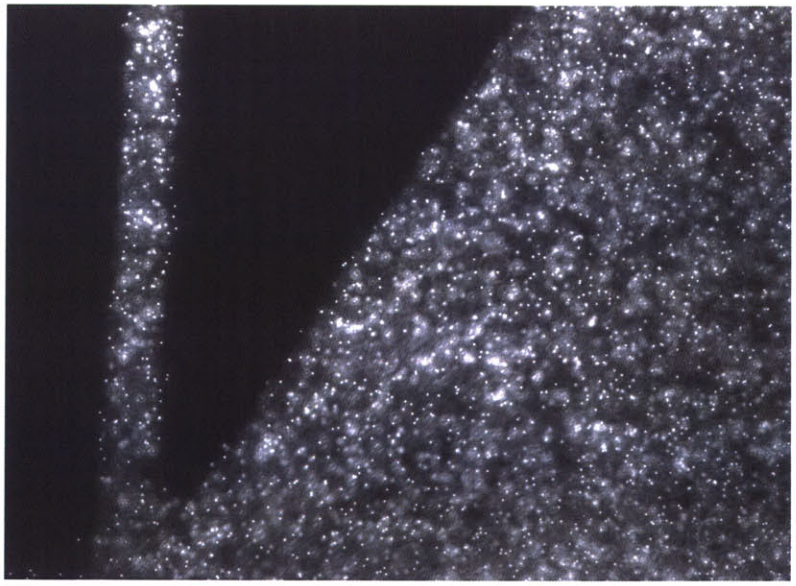

Figure 6.2.4: 100x magnification. Cross-channel of device in Figure 6.2.3 that has been primed with beads.

Figure 6.2.5 shows the exit region where a stream of beads joins a stream with no beads and the two streams drain from the device.

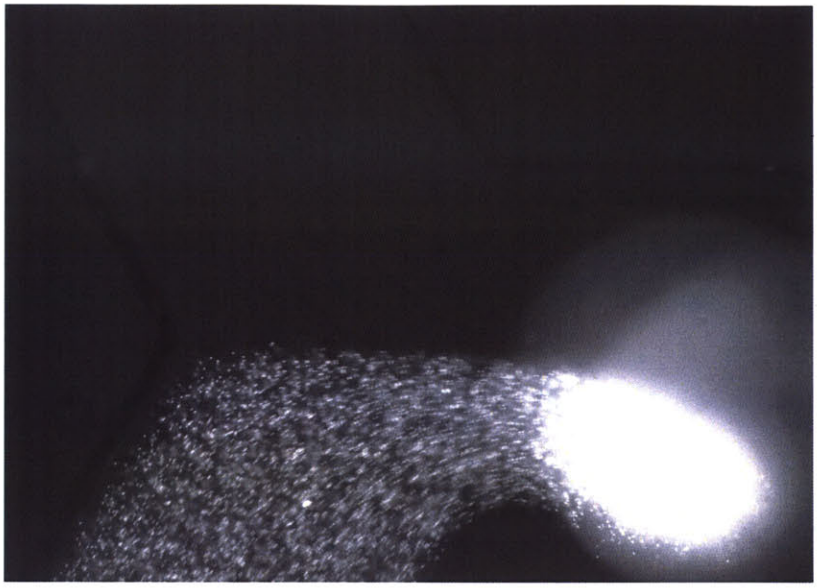

Figure 6.2.5: 100x magnification. Exit region of the device.

One of the major drawbacks of such a compact device is the difficulty in obtaining fluorescent images. Because the PDMS device is optically transparent, the stream carrying bulk fluid with a fluorescent tracer causes flooding of the cross-channel where diffusion is occurring. The inlets and outlets are also placed close to the cross-channel and have a stronger fluorescent signal than the cross-channel. While a gradient is readily observable in the cross-channel, these other sources of fluorescence introduce noise when trying to quantify the intensity of the gradient. Thus, another round of optimization is required to determine how far apart the inlets and outlets can be spaced such that they do not interfere with the imaging of the cross-channel.

6.3 Integrated Multilayer System

The following two figures show the results of the fabrication of the multi-layer geometry. Note the variability in the geometry and the general roughness of the edges. Also, the valves show a different degree of overlap/depression on the main channel, which can be correlated to their function.

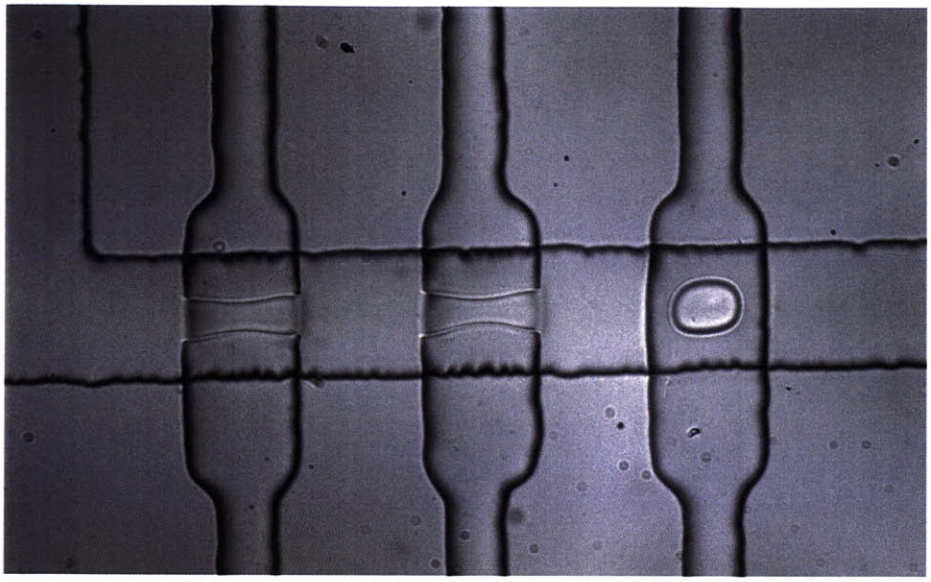

Figure 6.3.1: Image of 100 μm channel intersected by three 100 μm valves.

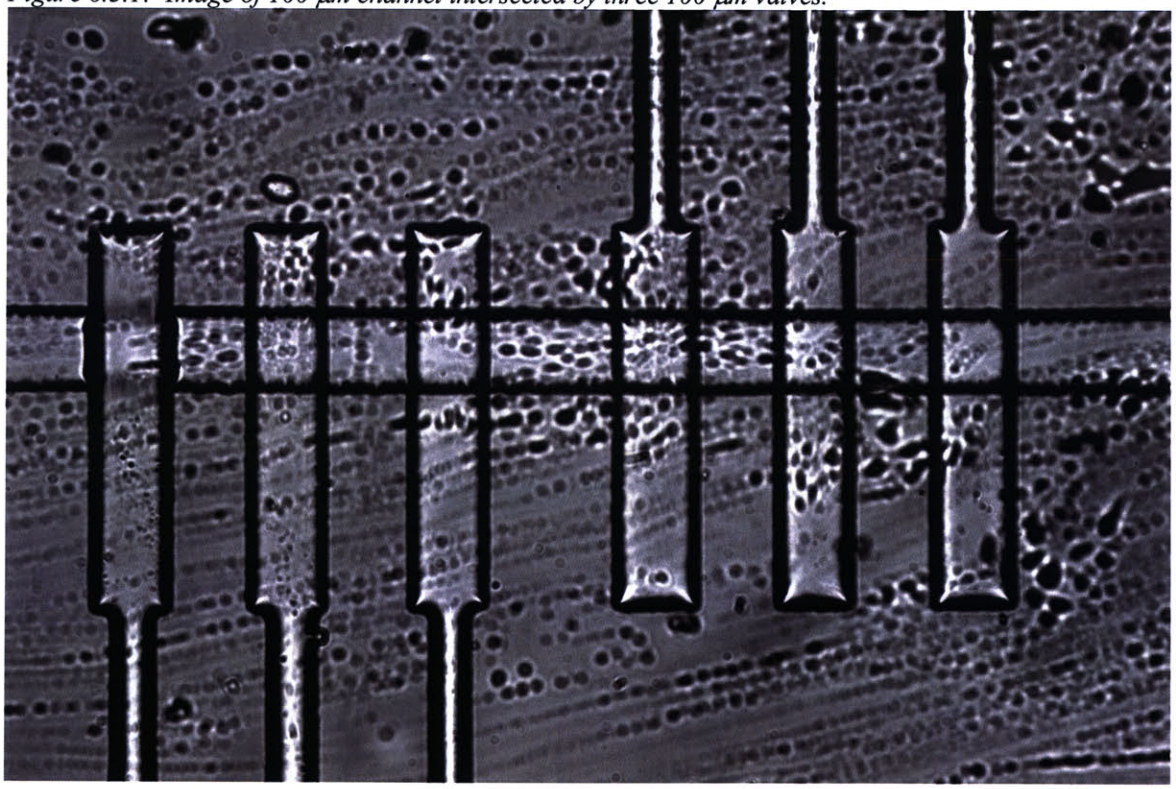

Figure 6.3.2: 6 100μm valves intersecting a flow channel. The first valve from the left is shown actuated.

Due to the variability in the fabrication outcome, the pressure that closes a valve must be calibrated for each device. Oftentimes a pressure of up to 30 psi is needed to initially close a

valve, as some of the features have become collapsed during the layer alignment process. The device can then resume operation at a lower pressure of ~10-15 psi. The pressure values reported here are approximate, based on an analog readout of the air valve regulator.

In order to visualize the flow, .51 μm and 1 μm fluorescent microspheres (Duke Scientific) diluted in water were pumped through the channels. The following image shows the flow through a peristaltic pump actuated in a 100, 110, 010, 011, 001, 101 pattern at a frequency of 100 Hz and a duty cycle of 0.5.

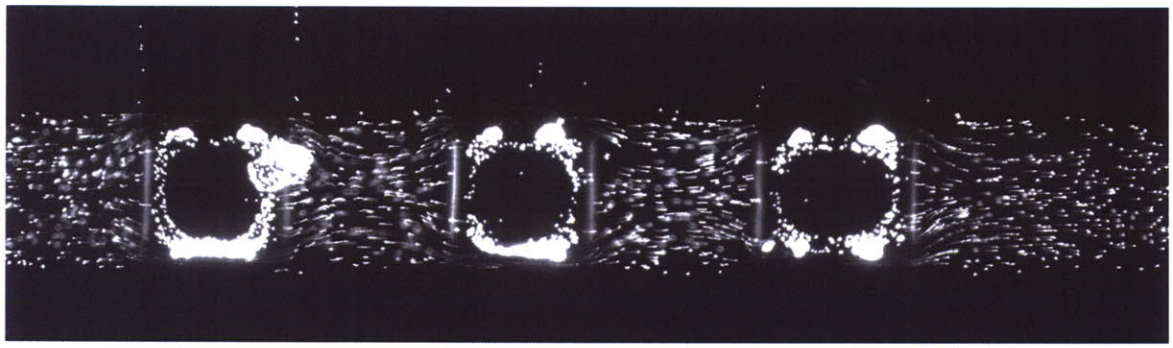

Figure 6.3.3: 1 μm fluorescent microspheres in peristaltic pump.

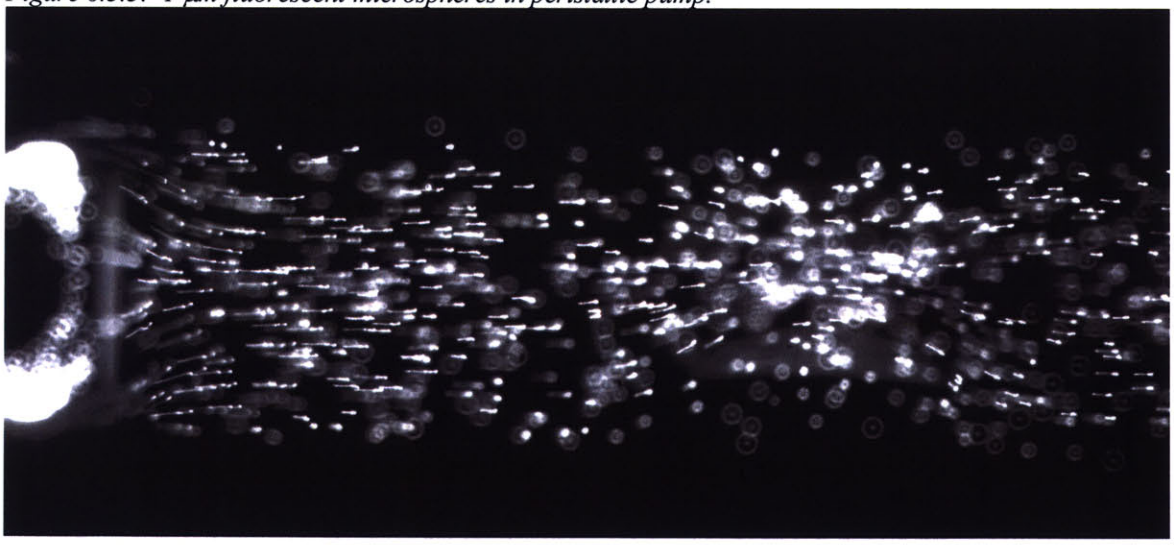

Figure 6.3.4: 1 μm fluorescent microspheres exiting peristaltic pump.

Some of the fabrication runs resulted in insufficiently rounded flow channels. The figure below shows the leakage that occurs through the sides of the valve when it is actuated.

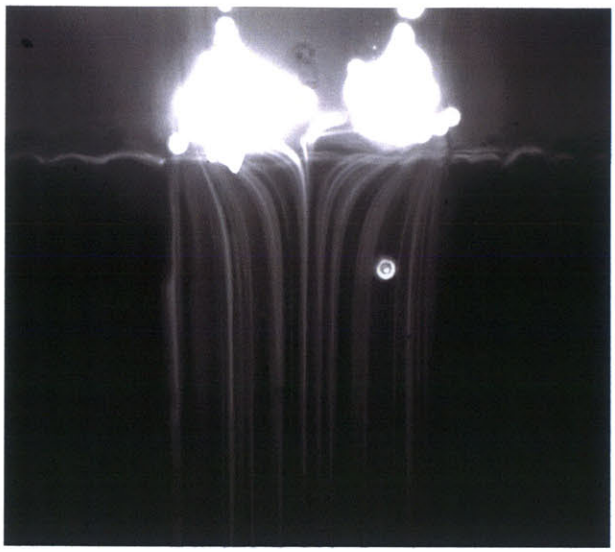

Figure 6.3.5: Leakage through the sides of the valve actuating a square channel as traced by 1 μm microspheres. Note: the bright spots in the image are a result of the fluorescent microspheres becoming embedded in the polymer during actuation.

6.4 Gradient

Although the fluorescent microspheres are neutrally buoyant, they are slow diffusing due to their large size. Therefore, we were unable to observe diffusion or gradients of microspheres in the chamber.

A rapidly diffusing fluorescent molecule, Rhodamine 110 was used to view gradients established through diffusion in the cross-channel. Rhodamine has a molecular weight of 366.80 and a coefficient of diffusion, $D \cong 4.37 \times 10^{10}\ m^2s^{-1}$. Rhodamine, therefore, travels at ~20 μm/s – a single molecule transversing a 10 mm cross-channel in ~8 minutes.

Figure 6.4.1 shows an image of a developing gradient of Rhodamine 110 across the length of a 50μm cross-channel. However, because individual rhodamine particles are not visible under the microscope, it is not possible to detect or measure slow flowrates in the cross-channel or use rhodamine to determine if the two parallel channels are balanced.

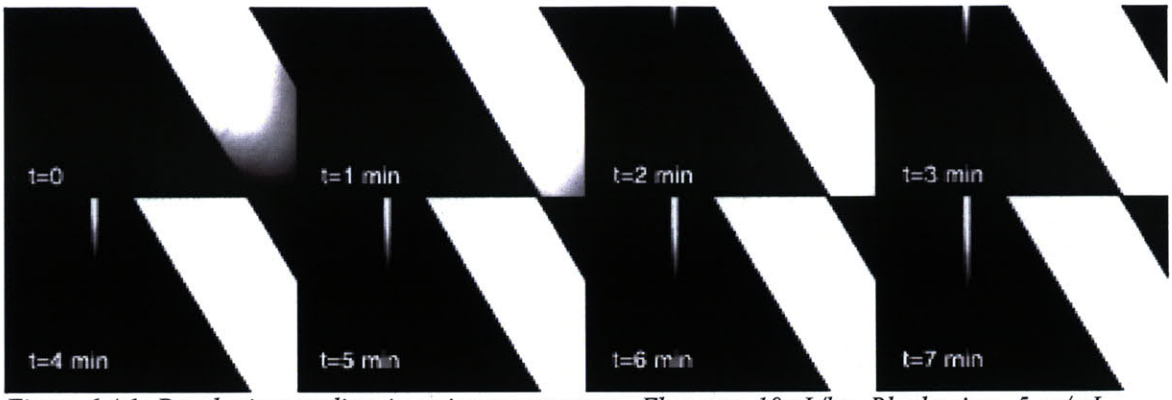

Figure 6.4.1: Developing gradient in syringe pump setup. Flowrate: 10 µL/hr. Rhodamine: .5 µg/mL Exposure time: 0.05 sec. Wavelength: 500 – 650 nm.

A combination of Rhodamine 110 and fluorescent microspheres was used to balance the flow between the two lines and observe a gradient in the cross-channel. The effect of microspheres in the flow on cells has not been investigated.

6.5 Cell Chemotaxis in Neutrophils

Cells loading through an inlet port proved unsuccessful, as even a gas-tight syringe could not provide a complete occlusion to flow. Due to the elastomeric properties of PDMS, leakage occurs at inlets where pins and tubing are inserted into the device. This should not be a problem in the multilayer device, as a valve can be closed at the inlet, thereby preventing cells from entering the main channels and allowing for a more precise placement of cells in the cross-channel.

Cells were, therefore, loaded into the channels through one of the inlet ports and allowed to settle and adhere for approximately 5 minutes. The following figure shows cells that have been loaded into the microchannels. The cross-channel, as well as the main channels, contains a dilute concentration of cells.

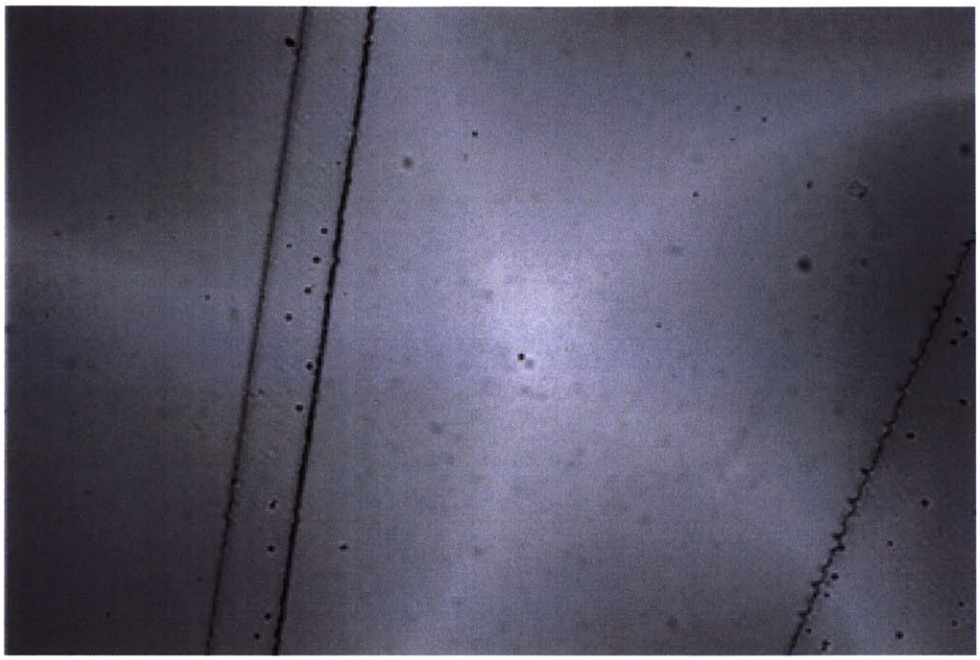

Figure 6.5: Mononuclear leukocytes in microchannels. The cross-channel is 50 μm wide.

When exposed to a .1M FMLP (Formal Met-Leu-Pro), cells were shown to move with a speed of approximately 20μm/second.

7.0 Discussion and Direction of Future Work

As of this writing, fabrication methodologies have been established, characterization of the chemotaxis chamber has been completed, and cell viability and chemotaxis in the chamber have been demonstrated. Constant volume flowrate created by a syringe pump has been used to establish temporally and spatially stable gradients in the chamber.

Another method shown effective for creating a stable gradient is gravity feed. An advantage of the gravity feed system is the low flowrate, and therefore low use of reagents. Its advantage is the relatively inexpensive and simple setup. Its drawback is the lack of accuracy with which a level of fluid can be maintained constant in the two syringes once the syringes have

been positioned. Another drawback is the inability to accurately calculate flowrates and velocities in the flow channel, whereas syringe pumping allows one to accurately predict velocities based on known volume flowrates. Knowing the velocities in the side channels, however, is not crucial to the experiment, as long as flow in the cell channel is non-existent.

However, the goal is to fabricate and integrated chamber that uses peristaltic pumps and valves to establish gradients and control the delivery of chemoattractant to the cells. Ultimately, the chamber will contain integrated modules for mixing of various concentrations of reagents and placing cells in designated areas. Effective mixing in microchannels has been demonstrated [20], [21], [17], [22].

In addition, rather than using a separate controller and temperature strip, the chamber may contain an embedded microfabricated temperature control element. Though many of the biology laboratories interested in using these methods to study chemotaxis may already have microscopes equipped with an environmental chamber for controlling temperature, oxygen and carbon dioxide levels, it may not be practical to fit the entire setup in such a chamber. Furthermore, having an integrated/embedded temperature control system would make for a more versatile device. The chamber can then be used to conduct many new and exciting chemotaxis experiments using a variety of cells including mutants and knock-outs for proteins involved in chemotaxis. The chamber can also be used to study competing gradients of several chemoattractants, start and stop flow from several reservoirs, and reverse the direction of the gradient.

Because the manufacturing of the pumps requires proper functioning of six independent valves and given the low throughput of the fabrication methods, the embedded peristaltic pumping may not prove to be the best option for creating flow in the chambers. If a gravity feed

or a syringe pumping method is adopted, a multilayer geometry may still be needed to create valves. As of this writing, we have only demonstrated proper functioning of 100x10 μm valves. These dimensions are inadequate to support experiments with endothelial cells because the cell dimensions are larger than the height of the channels. The Quake group has reportedly created PDMS valves of dimensions greater than 200x20 μm [personal communication with T. Thorsen].

In order to limit the need for scaling of the valves, while still maintaining the ratio of resistances between flow channels and cross-channel, and alternative geometry may be devised. Furthermore, endothelial cells move much slower than leukocytes (order of microns/hour). Therefore, the cross-channel can be shortened, thereby reducing diffusion times. Figure 7.1.1 shows a potential geometry that can be used with endothelial cells.

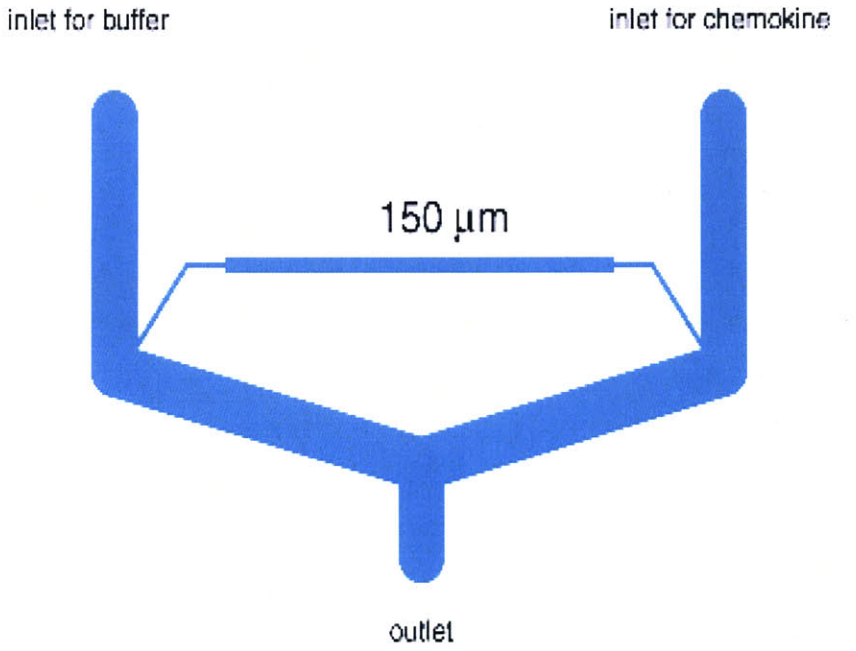

Figure 7.1.1: Proposed geometry for future devices.

To date, no quantifiable studies have been conducted exploring the effects of stable gradients on monolayers. While monocyte viability has been shown for a period of several

hours, such experiments have not been conducted for dividing cells such as endothelial cells. The first step to conducting experiments in monolayer chemotaxis would be to demonstrate that the chamber provides a suitable environment for cell growth division over the course of several days. Next, effects of competing chemoattractant and chemorepellant gradients could be observed.

Works Cited

1. Jeon, N.L., et al., *Neutrophil chemotaxis in linear and complex gradients of interleukin-8 formed in a microfabricated device.* Nature Biotechnology, 2002. **20**(8): p. 826-830.
2. Levchenko, A. and P.A. Iglesias, *Models of eukaryotic gradient sensing: application to chemotaxis of amoebae and neutrophils.* Biophys J, 2002. **82**(1 Pt 1): p. 50-63.
3. Iglesias, P.A. and A. Levchenko, *Modeling the Cell's Guidance System.* Science's STKE, 2002(148): p. 1-10.
4. Iikima, M., Y.I. Huang, and P. Devreotes, *Temporal and Spacial Regulation of Chemotaxis.* Developmental Cell., 2002. **3**: p. 469-478.
5. Zicha, D., G.A. Dunn, and A.F. Brown, *A new direct-viewing chemotaxis chamber.* J Cell Sci, 1991. **99 (Pt 4)**: p. 769-75.
6. Anderson, J.R., et al., *Fabrication of Topologically Complex Three-Dimensional Microfluidic System in PDMS by Rapid Prototyping.* Anal. Chem., 2000. **72**: p. 3158-3164.
7. Dertinger, S.K.W., et al., *Generation of Gradients Having Complex Shapes Using Microfluidic Networks.* Anal. Chem., 2001. **73**: p. 1240-1246.
8. Mao, H., P.S. Cremer, and M.D. Manson, *A sensitive, versatile microfluidic assay for bacterial chemotaxis.* PNAS, 2003. **100**(9): p. 5449-5454.
9. www.bioprotocolonline.com. May 15, 2003
10. McDonald, J.C. and G.M. Whitesides, *Poly(dimethylsiloxane) as a Material for Fabricating Microfluidic Devices.* Acc Chem Res, 2002. **35**(7): p. 491-9.
11. McDonald, J.C., et al., *Fabrication of microfluidic systems in poly(dimethylsiloxane).* Electrophoresis, 2000. **21**(1): p. 27-40.
12. Whitesides, G.M., et al., *Soft lithography in biology and biochemistry.* Annual Review of Biomedical Engineering, 2001. **3**: p. 335-373.
13. Madou, M.J., *Fundamentals of Microfabrication: The Science of Minituarization.* 2002(2): p. 342.
14. Unger, M.A., et al., *Monolithic microfabricated valves and pumps by multilayer soft lithography.* Science, 2000. **288**(5463): p. 113-116.
15. Thorsen, T., S.J. Maerkl, and S. Quake, *Microfluidic Large-Scale Integration.* Science, 2002. **298**: p. 580-584.
16. Unger, M., H.P. Chou, and T. Thorsen, *Monolithic Microfabricated Valves and Pumps by Multilayer Soft Lithography.* Science, 2000. **288**: p. 113-116.
17. Stroock, A.D., et al., *Chaotic mixer for microchannels.* Science, 2002. **295**(5555): p. 647-651.
18. Chaudhury, M.K. and G.M. Whitesides, *Correlation between Surface Free-Energy and Surface Constitution.* Science, 1992. **255**(5049): p. 1230-1232.
19. Albrecht, E. and H.R. Petty, *Cellular memory: neutrophil orientation reverses during temporally decreasing chemoattractant concentrations.* Proc Natl Acad Sci U S A, 1998. **95**(9): p. 5039-44.
20. Chou, H.P., M. Unger, and S. Quake, *A Microfabricated Rotary Pump.* Biomedical Microdevices, 2001(3): p. 323-330.
21. Jacobson, S.C., T.E. McKnight, and J.M. Ramsey, *Microfluidic devices for electrokinetically driven parallel and serial mixing.* Analytical Chemistry, 1999. **71**(20): p. 4455-4459.

22. Liu, R.H., et al., *Passive Mixing in a Three-Dimensional Serpentine Microchannel.* J MEMS, 2000. **9**(2): p. 190-197.

Appendix A: Spin Curves for Various Reagents Used in Fabrication

AZ4620 Spin Curve:

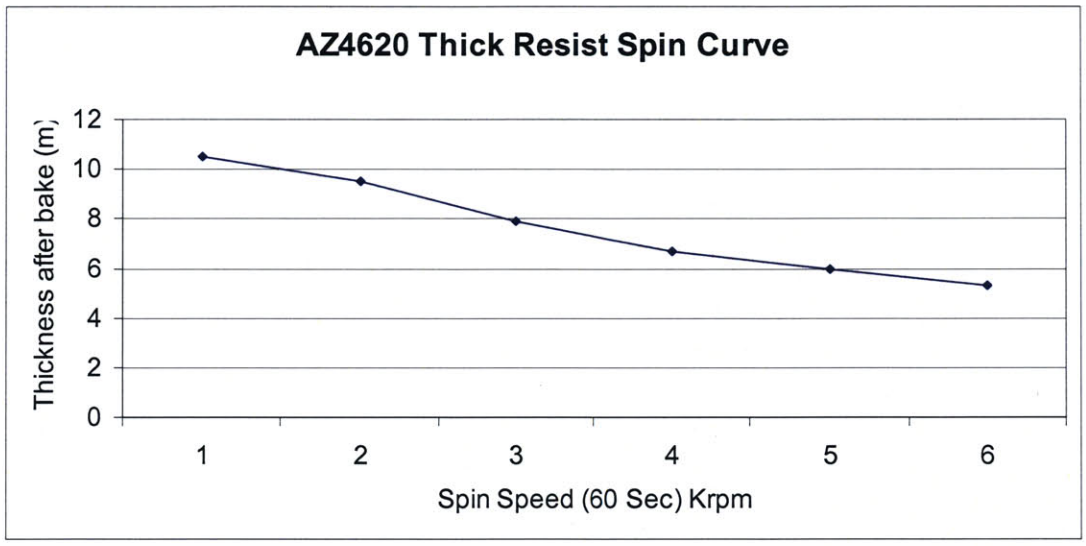

Source: http://www-mtl.mit.edu

PDMS Spin Curves
(courtesy of Mats Cooper)

Thickness vs Spin Time for 20:1 PDMS

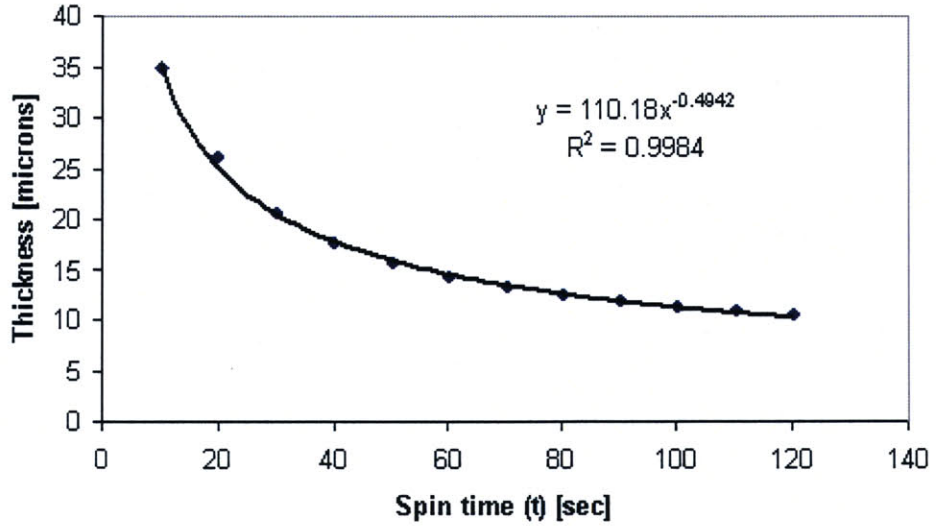

Thickness vs Spin Rate (for 30 sec spin time)

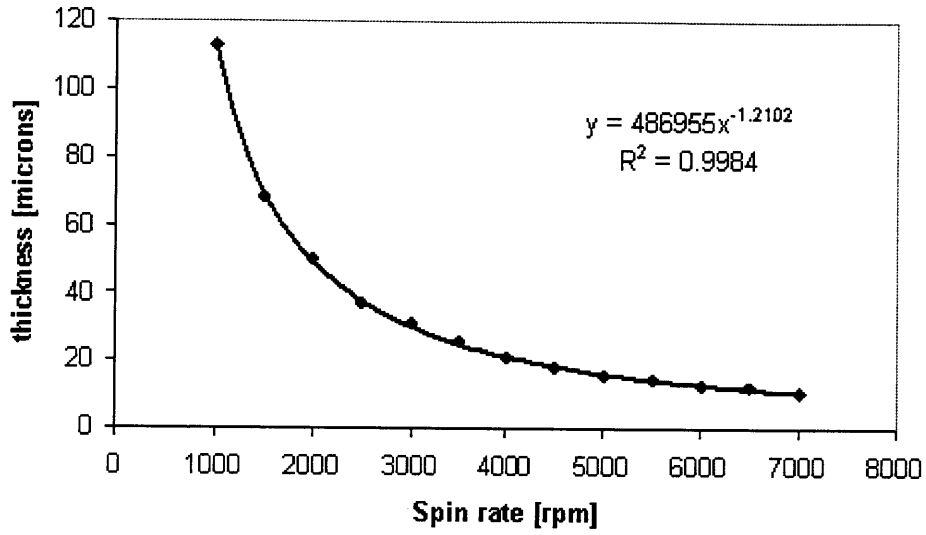

Appendix B: Selected Properties of SYLGARD® 184 Silicone Elastomer

Property	Value	hUnit
As supplied:	5500	mPa.s
Viscosity at 23°C (Base)		
Viscosity at 23°C, immediately after mixing with Curing Agent	4000	mPa.s
Cured 4 hours at 65°C:		
Mixing ratio by weight (Base:Curing Agent): 10:1		
Durometer hardness, Shore A	50	
Tensile strength	7.1	Mpa
Tear strength - die B	2.6	kN/m
Specific gravity at 23°C	1.05	
Coefficient of thermal conductivity	0.17	W/(m.K)

Source: http://www.dowcorning.com/DataFiles/090007b58001c0ae.pdf

Permeability of PDMS (Cured SYLGARD® 184 Silicone Elastomer)

The permeation rates of several gases and liquid vapors through PDMS elastomers are shown below. The numbers given represent cubic centimeters times 10 -9 of gas at normal temperature and pressure diffusing through one centimeter per second, per square centimeter, per centimeter of mercury pressure difference.

Gas	Permeability
N_2	25
CO_2	270
NO	50
NH_3	500
O_2	50
CO	30
H_2	55
NO_2	635
H_20	3000

Source: personal communication with Dow Chemical

Appendix C: Selected Properties of Rhodamine Dyes

The peak excitation and emission wavelengths of rhodamine 110 are 498 nm and 521 nm, respectively.

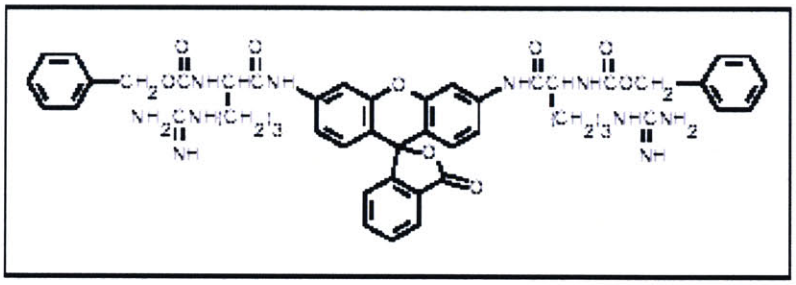

Figure C.1: Chemical structure of the bis-(CBZ-L-arginine amide) derivative of rhodamine 110 (R-6501).

Appendix D: SolidWorks Drawing of Air Manifold

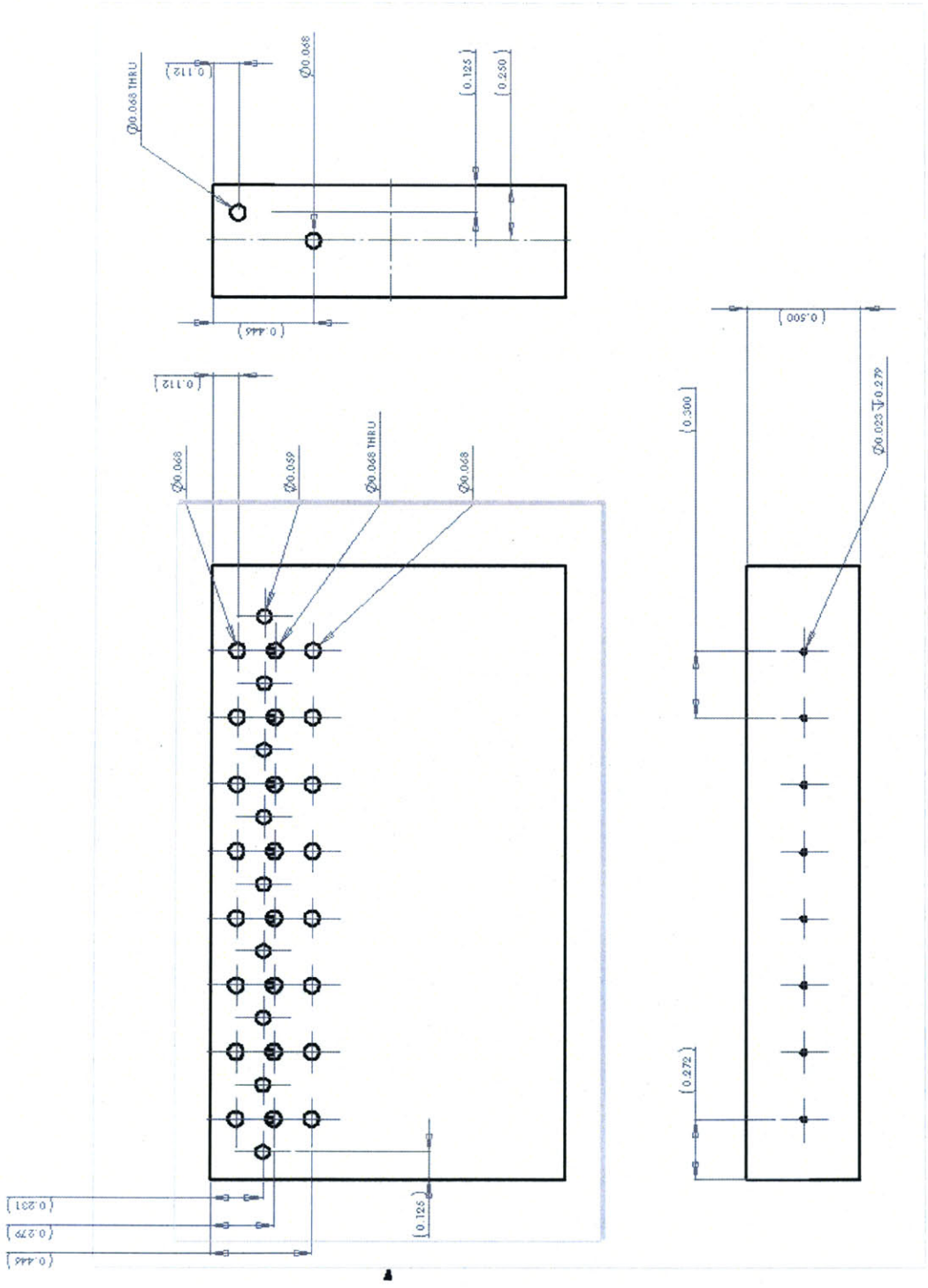

Appendix E: Controller Board Electronics

DigiKey		
CP-102A-ND	CONN JACK POWER 2.1MM PCB	$0.38
A26510-ND	CONN HDR BRKWAY .100 40POS RT/A	$1.20
AKC50G-ND	CONN IDC SOCKET 50POS W/POL 15AU	$1.57
2-174225-5-ND	CONN HDR PLUG D-SUB RTANG 68 POS	$20.19
OD102J-ND	RESISTOR 1.0K OHM .25W CARB COMP	$0.42
1N4005DICT-ND	RECTIFIER GPP 600V 1A DO-41	$0.13
Mouser		
610-2N3053	2N3053 TO-39 NPN Transistor	$0.67
National Instruments		
777314-01	PCI-DIO-32HS and NI-DAQ for WinXP	$995
183432-01	SH68-68-D1 Shielded Cable, 1 m	$ 125